NASA TECHNICAL NOTE

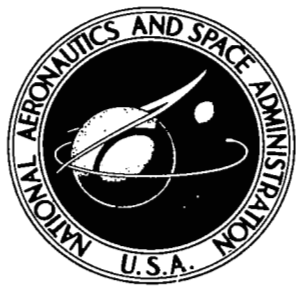

NASA TN D-6321

MEASUREMENTS OF BOUNDARY LAYER TRANSITION, SEPARATION AND STREAMLINE DIRECTION ON ROTATING BLADES

by William J. McCroskey

Ames Research Center

and

U.S. Army Air Mobility R&D Laboratory
Moffett Field, Calif. 94035

NATIONAL AERONAUTICS AND SPACE ADMINISTRATION • WASHINGTON, D. C. • APRIL 1971

1. Report No.	2. Government Accession No.	3. Recipient's Catalog No.
NASA TN D-6321		

4. Title and Subtitle	5. Report Date
MEASUREMENTS OF BOUNDARY LAYER TRANSITION, SEPARATION AND STREAMLINE DIRECTION ON ROTATING BLADES	April 1971
	6. Performing Organization Code

7. Author(s)	8. Performing Organization Report No.
William J. McCroskey	A-3863
	10. Work Unit No.
	721-60-10-02-00-21

9. Performing Organization Name and Address	11. Contract or Grant No.
NASA Ames Research Center and U.S. Army Air Mobility R&D Laboratory Moffett Field, Calif., 94035	
	13. Type of Report and Period Covered
12. Sponsoring Agency Name and Address	Technical Note
National Aeronautics and Space Administration Washington, D. C. 20546	14. Sponsoring Agency Code

15. Supplementary Notes

Edited by NASA Ames Research Center

16. Abstract

Laminar separation, transition to turbulence, and surface streamline directions were measured on belicopter rotor blades in a variety of rotating and nonrotating configurations. The results indicate that the centrifugal effects of rotation do not signficantly alter the boundary layer development for most operating conditions. Laminar separation bubbles were observed near the leading edge of the upper surface of the blades at moderate and large angles of attack, and this phenomenon triggered a sudden transition to turbulent flow. Surface streamline patterns were found to be the same for both laminar and turbulent flows.

17. Key Words (Suggested by Author(s))

Rotating blades
Helicopter boundary layers
Laminar separation
Transition
Streamline direction
Centrifugal pumping
Flow visualization

18. Distribution Statement

Unclassified - Unlimited

19. Security Classif. (of this report)	20. Security Classif. (of this page)	21. No. of Pages	22. Price*
Unclassified	Unclassified	41	$3.00

*For sale by the National Technical Information Service, Springfield, Virginia 22151

TABLE OF CONTENTS

SYMBOLS

c	chord, m
d	chordwise offset distance between the leading edge and the axis of rotation, m
R	rotor radius, m
Re	Reynolds number based on chord length and chordwise component velocity at the blade tip
V	forward flight velocity
x	coordinate along the chord line
$\bar{x}$	coordinate along the blade surface
y	coordinate normal to the chord line
α	local aerodynamic angle of attack in the chordwise direction, deg
θ	collective pitch angle, deg
Λ	yaw angle, deg
μ	tip speed ratio, $\Omega d/\Omega R$ or $V_\infty/\Omega R$
ψ	azimuth angle of the blade span axis relative to the forward flight direction, deg
Ω	rotor speed, rpm

Subscripts

S	separation
T	transition

MEASUREMENTS OF BOUNDARY LAYER TRANSITION, SEPARATION AND STREAMLINE DIRECTION ON ROTATING BLADES

William J. McCroskey

Ames Research Center
and
U.S. Army Air Mobility Research and Development Laboratory

SUMMARY

Laminar separation, transition to turbulence, and surface streamline directions were measured on helicopter rotor blades in a variety of rotating and nonrotating configurations. The results indicate that the centrifugal effects of rotation do not significantly alter the boundary layer development for most operating conditions. Laminar separation bubbles were observed near the leading edge of the upper surface of the blades at moderate and large angles of attack, and this phenomenon triggered a sudden transition to turbulent flow. Surface streamline patterns were found to be the same for both laminar and turbulent flows.

INTRODUCTION

Contemporary efforts to improve the performance of V/STOL aircraft have spawned an increasing interest in understanding the role of viscous effects in these applications. Despite the importance of aerodynamic drag and boundary layer separation characteristics in determining the limits of satisfactory operation of rotating lifting surfaces, the actual nature of the viscous flow remains virtually unknown. Therefore the U.S. Army Air Mobility Research and Development Laboratory has undertaken a long-range study concerning the fundamental nature of boundary layer flows on rotors and propellers and how these boundary layers may differ from the more familiar two-dimensional viscous flows around translating bodies. This report describes some of the initial experimental results from the first phase of that program.

This preliminary investigation dealt with the location of laminar separation bubbles and the transition from laminar to turbulent flow on rotating helicopter blades, and with directions of the boundary layer streamlines at the blade surfaces. The first objective was to determine the effects of rotation and spanwise flow due to forward flight upon laminar separation and transition. This is an important practical question relating primarily to skin-friction drag and, to a lesser extent, to stall phenomena. The second objective was to determine whether the effects of rotation and crossflow due to forward flight are fundamentally different for laminar and turbulent boundary layers with the same inviscid flow. This is important with regard to the emphasis that should be placed in the future upon laminar boundary layer theories, which are considerably easier to develop than turbulent ones.

A complete description of the viscous boundary layer on a helicoper rotor blade in forward flight would encompass three-dimensional unsteady flow with compressibility and rotational effects present, coupled with an extremely complex potential flow field. Such a description is well beyond the capabilities of contemporary boundary layer analyses, but it is possible to build upon what is known about simpler two- and three-dimensional flows with the aid of figure 1. The scope of the present investigation is limited to the four steady configurations depicted in figure 1, excluding the complete problem illustrated in the lower right hand corner of the figure. In the following sections, the primary emphasis will be placed on the transition and surface flow direction patterns.

The present experiments are direct extensions of those reported by Tanner and Yaggy (ref. 1), and Velkoff, Blaser, and Jones (ref. 2) in both scope and methodology. A unique aspect of the present investigation is the use of a hovering rotor with offset blades shown in the lower left hand corner of figure 1. This was proposed by McCroskey and Yaggy (ref. 3) for studying the strong three-dimensional effects of forward flight without the complications of unsteady aerodynamics.

DESCRIPTION OF THE EXPERIMENTS

The tests utilized the untwisted blades described in table 1. These were tested in a 7- by 10-foot wind tunnel as fixed wings, as shown in figure 2, and on static propeller test stands, as shown in figures 3 and 4. Blades of series 1 and 2 were used primarily to obtain results for laminar separation. These separation studies were patterned after those of Velkoff et al. (ref. 2), in which ammonia vapor was emitted from orifices and allowed to develop a pattern on ordinary ozalid blueline reproduction paper attached to the blade.

Typical test results are shown in figure 5 for ammonia orifices located at the leading edge and at $x/c \approx 0.2$. The trace on the left indicates an abrupt change in flow direction just downstream of the point where the suction peak in the chordwise pressure distribution would be expected to occur. The ammonia trace in the center of figure 5 shows a strong radial outflow and indicates some reversed flow. The picture of the flow is made more complete by considering the oscilloscope traces of hot wire anemometers placed near the outer edge of the boundary layer, also shown in figure 5. The hot wire signal from the immediate vicinity of the ammonia trace discontinuities shows the irregular fluctuations that characterize locally disturbed flow; elsewhere, the signals are relatively calm. The combined information in figure 5 implies that a laminar separation bubble exists just downstream of the local suction peak and that turbulent reattachment occurs afterwards, very similar to the boundary layer behavior on two-dimensional airfoils.

Blades of series 3 and 4 were borrowed from the Bell Helicopter Company and were used to determine the streamwise transition patterns. The series 4 blades were originally used in the study reported by Tanner and Yaggy (ref. 1). Additional tests were performed on these and on the thinner series 3 blades having the airfoil geometry shown in figure 6. The leading edge portion of the series 3 blades was approximately equivalent to an NACA 0012 profile, and the rear portion was flat with a trailing edge thickness of 1.27 mm (0.05 in.). The blades were mounted in the wind tunnel and on a propeller test stand, as shown in figures 2 and 3, respectively. These blades were tested with and without boundary layer trips that were made of serrated masking tape placed very near the leading edge.

Flow visualization on the series 3 and 4 blades was obtained by means of a subliming film of acenapthane which produced surface patterns such as those shown in figure 7.[1] The darker areas correspond to higher rates of sublimation of the white film from the black blade surface; this effect can be seen in the high-shear laminar region very near the leading edge and in the turbulent region at the rear portion of the blade. Thus the intermediate laminar region of reduced sublimation appears white until the flow becomes turbulent. The dark fan-like patterns originating near the leading edge were produced by small unintentional disturbances on the surface of the blade and approximately indicate the surface streamline directions. This use of the acenapthane sublimation to determine the location of transition was verified by observing the dynamic response of five heated-film skin-friction gages, following the method of Bellhouse and Schultz (ref. 5), and by the use of oil streaks, as shown in figure 7. The thin black oil streaks were centrifuged outward as well as dragged by the airflow. They show an abrupt change in direction at each laminar-turbulent interface, due to the changes in the shear stress acting on the oil bead as it traverses the interface; the oil bead trajectory is more nearly chordwise in the turbulent regions.

Series 1 and 2 blades were tested only in rotation, with no offset, at rotational speeds from 400 to 1,000 rpm, giving maximum Reynolds numbers of about 1.4×10^5, based on tip speed and blade chord. Blades of series 3 and 4 were tested statically at free-stream velocities varying from 34 to 100 m/s (110 to 320 ft/s) in the wind tunnel and on the propeller stand at rotational speeds from 400 to 1,000 rpm. The rotational data presented in this report were obtained at approximately 600 rpm for which the tip speed and maximum Reynolds numbers were approximately 80 m/s (260 ft/s) and 1.4×10^6, respectively. Angles of attack and collective pitch angles were varied from zero through stall, and the sweep angle in the wind tunnel varied from 0 to $\pm 60°$. The offset distances from the leading edge of the blades to the axis of rotation were 0, -0.076, and ± 0.64 m (0, -2.5, and ± 21 in.), representing hover and $\mu = 0.42$ with $\psi = 0$ and 180°.

All of the data reported herein were obtained at spanwise stations between 60 and 80 percent of the blade tip radius. In this range, transition and separation were found to be essentially independent of spanwise location.

TRANSITION AND LAMINAR SEPARATION RESULTS

Static Blade, Zero Yaw

Tests of a nonrotating blade at zero yaw angle provided a frame of reference for the yawed and rotating blade tests. The effects of angle of attack on the location of transition are shown in figure 8, for several Reynolds numbers. Data from the series 4 blades, including those of Tanner and Yaggy (ref. 1), are summarized by the crosshatching.

The general trends of the transition data follow the expected behavior of the chordwise pressure gradients on the blade. That is, transition on the upper surface moved closer to the leading edge when the angle of attack was increased, just as the location of the maximum adverse pressure gradient would be expected to move forward. The differences in transition locations on the upper surfaces of the series 3 and 4 blades can be attributed to the differences in the two airfoil sections.

[1] This particular photograph was obtained by G. G. Morehouse in connection with the study reported in reference 4.

Yawed Static Blade

The transition data for the series 3 blades at various yaw angles and a free-stream Reynolds number of 0.61×10^6/m (2×10^6/ft) are displayed in figure 9. Upper surface data at lower unit Reynolds numbers, which are not shown, were not significantly different. On the lower surface, transition seemed to move closer to the leading edge as the yaw angle was increased. In contrast with most of the test conditions, the lower surface transition lines were somewhat ambiguous at high values of Λ and α. Below the stall angle, the location of transition on the upper surface still seems to follow the expected trends of the chordwise pressure distribution, which would theoretically be independent of yaw angle.

Rotating Blade in Conventional Hover

The variation in transition point location with collective pitch is shown in figure 10 for the series 3 blades for small values of d/R. Series 4 data are shown for comparison. For these conditions, the inflow through the rotor reduced the local aerodynamic angle of attack to roughly half the geometric pitch angle, θ.

The unstalled hover transition data behaved essentially the same as the nonrotating data, in agreement with the results of Tanner and Yaggy (ref. 1). As before, the differences between the series 3 and 4 results can be attributed to the differences in the airfoil sections.

The measured location of the laminar separation, the location of the abrupt change in the flow direction (cf. fig. 5), is plotted in figure 11. The data of Velkoff et al. (ref. 2) are also shown in figure 11(b). The separation point moved forward with increasing collective pitch, reflecting the change in the chordwise pressure distribution that would accompany the change in angle of attack. The results appear to be independent of Reynolds number over the range investigated.

Rotating Blade With Large Offset

The configuration shown in figure 4 provides the large local sweep angles encountered in forward flight at $\mu = |\pm d/R| = 0.42$ and $\psi = 0, 180°$, respectively,[2] without the complications of unsteady aerodynamics. However, the data of figure 12 show that the transition location was not greatly affected by this crossflow.

FLOW DIRECTION AND STALL ONSET

The acenapthane sublimation patterns that were obtained under a variety of configurations and conditions provided qualitative information about flow directions in the boundary layer. In this phase of the investigation, the flow patterns were observed on both surfaces of the blades. On the lower surface, observations were made with and without a boundary-layer trip, to compare the crossflow in laminar and turbulent boundary layers subjected to identical pressure gradients and centrifugal accelerations.

[2] When $d > 0$, the leading edge of the blade is ahead of the axis of rotation, and the crossflow is outward along the span, corresponding to $\psi = 0$ in conventional helicopter flight.

Yawed Static Blade

The acenapthane pattern on a nonrotating series 3 blade at large yaw angle is shown in figure 13. Also visible are the heated-film skin-friction gages whose fluctuating signals were used to verify the acenapthane indications of transition.

There are slight curvatures in the wake patterns behind the disturbance elements, but the streamline directions generally followed the tunnel free-stream direction very closely. As long as the blade was not stalled, this general behavior was observed over the entire range of α, Λ, and Re.

Rotating Blade, No Offset

The patterns on the series 3 blades corresponding to conventional hover are shown in figure 14 for small and moderate angles of attack. The most striking feature of all these patterns is their marked similarity. Excluding the tip region, the streamlines fell just inside of the circular arc representing an undisturbed-flow streamline. This occurred on both the upper and lower surfaces, and on the lower surface there was no measurable difference between the flow direction in laminar and turbulent flows.

Rotating Blade With Large Offset

The acenapthane patterns for large positive offset (approximating $\psi = 0°$ at $\mu = 0.42$) are shown in figure 15 and for negative offset ($\psi = 180°$, $\mu = 0.42$) in figure 16. As in the cases with no offset, the streamlines tended to lie just inside of circular arcs, and the streamline direction was the same whether the flow was laminar or turbulent.

Onset of Stall

Unfortunately, the acenapthane did not sublime in readily identifiable patterns when the boundary layer separated appreciably. However, the well-known behavior of the chordwise stall angle increasing with yaw angle was observed in the nonrotating tests.

Another interesting set of results was obtained by varying the offset distance while keeping the collective pitch fixed at a value near the onset of stall. The patterns so obtained are shown in figure 17, and a plot of the rotor torque at this and lower values of θ is shown in figure 18.

For $\theta = 22°$, d = 0, and $\Omega = 550$ rpm, the series 3 blades appeared to be just on the verge of stall, based on the acenapthane pattern shown in figure 17 and the sound level of the rotor. With positive offset (outward crossflow), the blades were not stalled at $\theta = 22°$. However, with negative offset and $\theta = 22°$, the flow pattern broke down completely, and the torque of the rotor and the sound level increased considerably, indicating that the blades were stalled.

It is interesting to note that this trend of stall delay or enhancement with changing offset runs counter to the predictions of the laminar analyses of Liu (ref. 6) and Dwyer and McCroskey (ref. 7) for infinite-span blades with constant circulation. In the experiment, of course, the boundary layer

was mostly turbulent, the circulation varied along the span, and the tips may have had a profound influence upon the onset of stall. Also, the analyses were carried out for smaller angles of attack, where the relative importance of the crossflow-induced apparent pressure gradient term ($W_e(\partial W_e/\partial x)$ in the notation of ref. 7) may have been significantly different.

DISCUSSION OF RESULTS

The most distinguishing feature of all of the experimental results described in the preceding sections is the striking similarity between the rotating and nonrotating behavior. The transition seemed to occur at approximately the same chordwise position in all cases. Also, the flow direction in the boundary layer, whether laminar or turbulent, appeared to follow very closely a hypothetical line representing the undisturbed flow. The only exceptions to the latter statement occurred very near the tip, in a small region associated with a laminar separation bubble, and when the flow was stalled or nearly so.

The apparent unimportance of rotational effects strongly suggests that all of the viscous flows investigated were dominated by the nature of the potential flow field and, in particular, by the chordwise pressure distribution. This lends considerable credence to the use of the "small-crossflow approximation" in boundary layer analyses. The similarity between laminar and turbulent streamline directions indicates that laminar theories can be used to enhance basic understanding of flows on rotors and propellers.

Further interesting insights and conclusions can be drawn from a composite graph of the transition and separation results, shown in figure 19. For rotating data in this figure, the angle of attack was calculated using simple blade-element momentum theory. Also shown in figure 19 are the results of a detailed numerical calculation of the laminar boundary layer, reported recently by Dwyer and McCroskey (ref. 7).

One of the most important points to be made in connection with figure 19 is that the chordwise pressure gradients are so strong at large angles of attack that the theoretical effects of crossflow and rotation in the short stretch of laminar flow are insignificant. Thus the numerical and experimental results for separation agree well with the two-dimensional calculations for large α. The laminar data appear to be independent of Reynolds number in agreement with theory and with two-dimensional experiments such as those of Gault (ref. 8).

Another important result is that the transition process for $\alpha \gtrsim 6°$ seems to occur in the free shear layer that develops after laminar separation, followed by turbulent reattachment shortly downstream. This hypothetical flow picture for moderate and high Reynolds numbers (e.g., greater than about 200,000) corresponds directly to the well-known separation bubble on two-dimensional airfoils, and it is sketched on the right side of figure 19. At lower angles of attack, however, transition to turbulence precedes, and therefore precludes, laminar separation, as indicated in the sketch on the left. This also occurs on the lower surface of the airfoil at all angles of attack.

CONCLUDING REMARKS

The boundary layer experiments of the present investigation indicate that for the suction surface of typical helicopter rotors, the transition from laminar to turbulent flow is dominated by the chordwise adverse pressure gradient and a conventional laminar separation bubble, rather than by Reynolds number, rotational, or crossflow effects. The results also indicate that the crossflow in the unseparated boundary layer is small with respect to the undisturbed potential flow streamlines, whether flow is laminar or turbulent. Therefore, the boundary-layer flow on a wide class of rotating blades bears a marked resemblance to its counterpart on conventional wings.

There are, of course, some significant differences in rotor and fixed-wing boundary layers. Though unimportant in a practical sense, centrifugal forces move the fluid significantly outward in separated regions, such as the laminar separation bubble or in trailing-edge separated flow. On the more practical side, high-aspect ratio helicopter rotors in forward flight and low aspect ratio propeller blades are known to develop much greater thrust without stalling than would be expected on the basis of two-dimensional boundary-layer behavior. This investigation completely ignored any unsteady effects, and little was learned about the actual mechanisms of stall on the rotating blades. These appear to be the areas of research that should now be emphasized.

What the present investigation, combined with the theoretical studies of reference 7, has provided is a much better basic understanding of the laminar flow on contemporary helicopter rotors and some initial insight into the nature of the turbulent flow. Purely rotational effects appear to be relatively unimportant, and the major three-dimensional and unsteady effects on the stall characteristics of actual rotors probably occur in the turbulent and separated regions of the boundary layer.

Since the laminar flow on the upper surface separates so near the leading edge for large α, the correct flow model apparently is a small region of essentially two-dimensional quasi-steady laminar flow, followed by a three-dimensional unsteady turbulent flow. This turbulent boundary layer has its starting or initial conditions in the x-direction determined by a classical short separation bubble and its subsequent behavior predominantly influenced by the chordwise pressure distribution. Another important feature is that the boundary layer crossflow is largely determined by the spanwise flow at the outer edge of the boundary layer, which is approximately $V_\infty \cos \psi$ in high-speed forward flight. This new knowledge, it is hoped, will serve as a useful guide for further theoretical and experimental investigations.

Ames Research Center
National Aeronautics and Space Administration
and
U.S. Army Air Mobility R&D Laboratory
Moffett Field, Calif. 94035, Jan. 18, 1971

REFERENCES

1. Tanner, W. H.; and Yaggy, P. F.: Experimental Boundary Layer Study on Hovering Rotors. J. Amer. Helicopter Soc., vol. 11, no. 3, 1966, pp. 22–37.

2. Velkoff, H. R.; Blaser, D. A.; and Jones, K. M.: Boundary Layer Discontinuity on a Helicopter Rotor Blade in Hovering. AIAA Paper 69–197, 1969.

3. McCroskey, W. J.; and Yaggy, P. F.: Laminar Boundary Layers on Helicopter Rotors in Forward Flight. AIAA J., vol. 6, no. 10, Oct. 1968, pp. 1919–1926.

4. Spivey, W. A.; and Morehouse, G. G.: New Insights Into the Design of Swept-Tip Rotor Blades. Amer. Helicopter Soc. preprint 420, June 1970.

5. Bellhouse, B. J.; and Schultz, D. L.: Determination of Mean and Dynamic Skin Friction, Separation and Transition in a Low Speed Flow With a Thin-Film Heated Element. J. Fluid Mech., vol. 14, pt. 2, Feb. 1966, pp. 379–400.

6. Liu, S. W.: The Laminar Boundary-Layer Flow on Rotating Cylinder. AFOSR TN 57–298, pts. 1 and 2, June 1957.

7. Dwyer, H. A.; and McCroskey, W. H.: Crossflow and Unsteady Boundary-Layer Effects on Rotating Blades. AIAA Paper 70–50, 1970.

8. Gault, D. E.: An Experimental Investigation of Regions of Separated Laminar Flow. NACA TN 3505, 1955.

TABLE 1.– DESCRIPTION OF MODEL ROTOR BLADES

Blade	Airfoil section	Rotor diameter		Chord		Instrumentation	Measured variable
		m	in.	m	in.		
1	NACA 0012	0.91	36	0.063	2.5	Hot wires Ammonia-azo Acenapthane	Separation point Transition point
2	NACA 0015	1.17	46	0.076	3	Ammonia-azo	Separation point
3	10 percent thickness 0012 L.E. radius	2.65	104	0.254	10	Skin friction gage Acenapthane	Transition point Streamline direction
4	NACA 0015	2.54	100	0.211	8.3	Acenapthane	Transition point Streamline direction

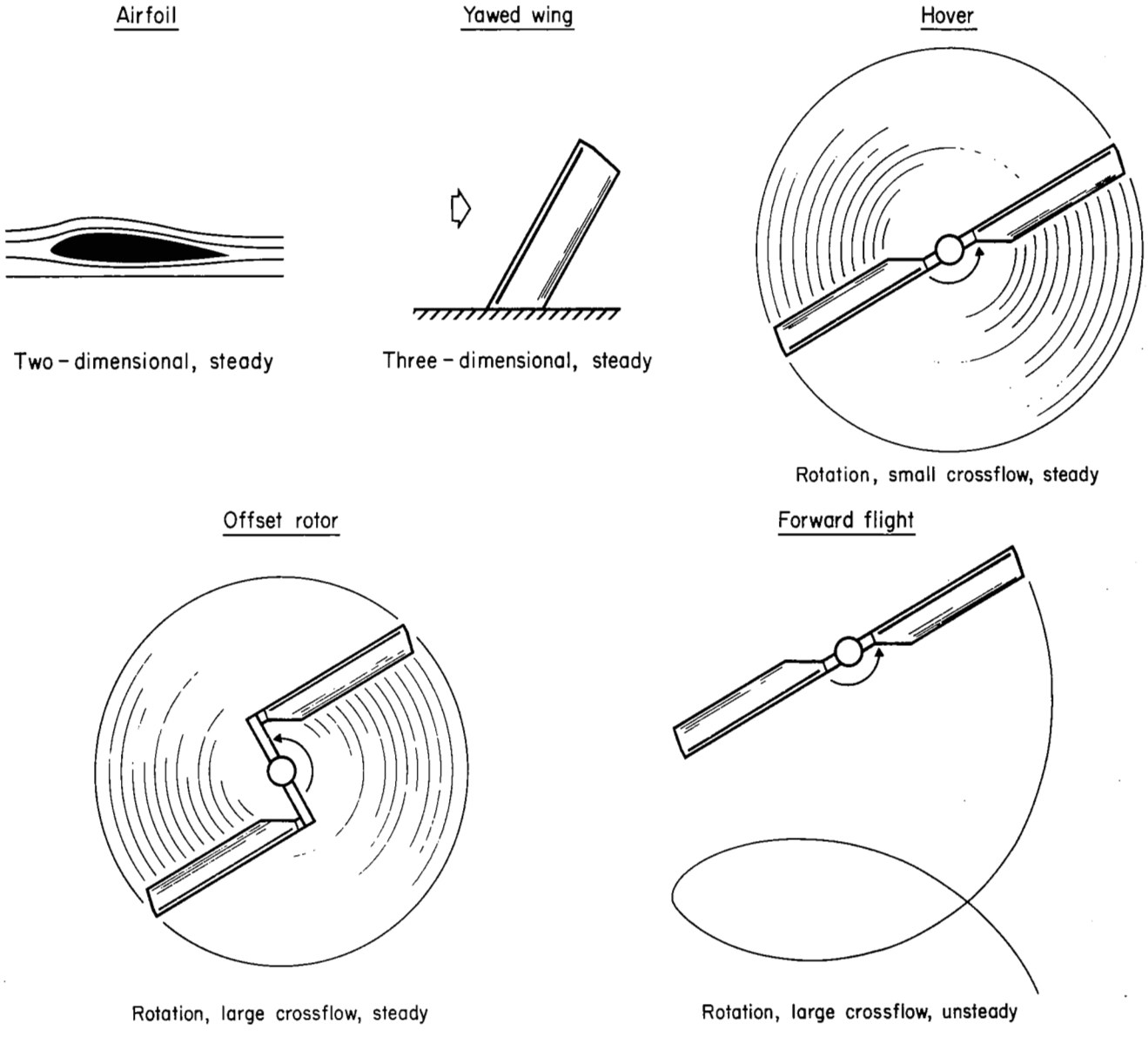

Figure 1.– Development of helicopter blade aerodynamics from simpler cases.

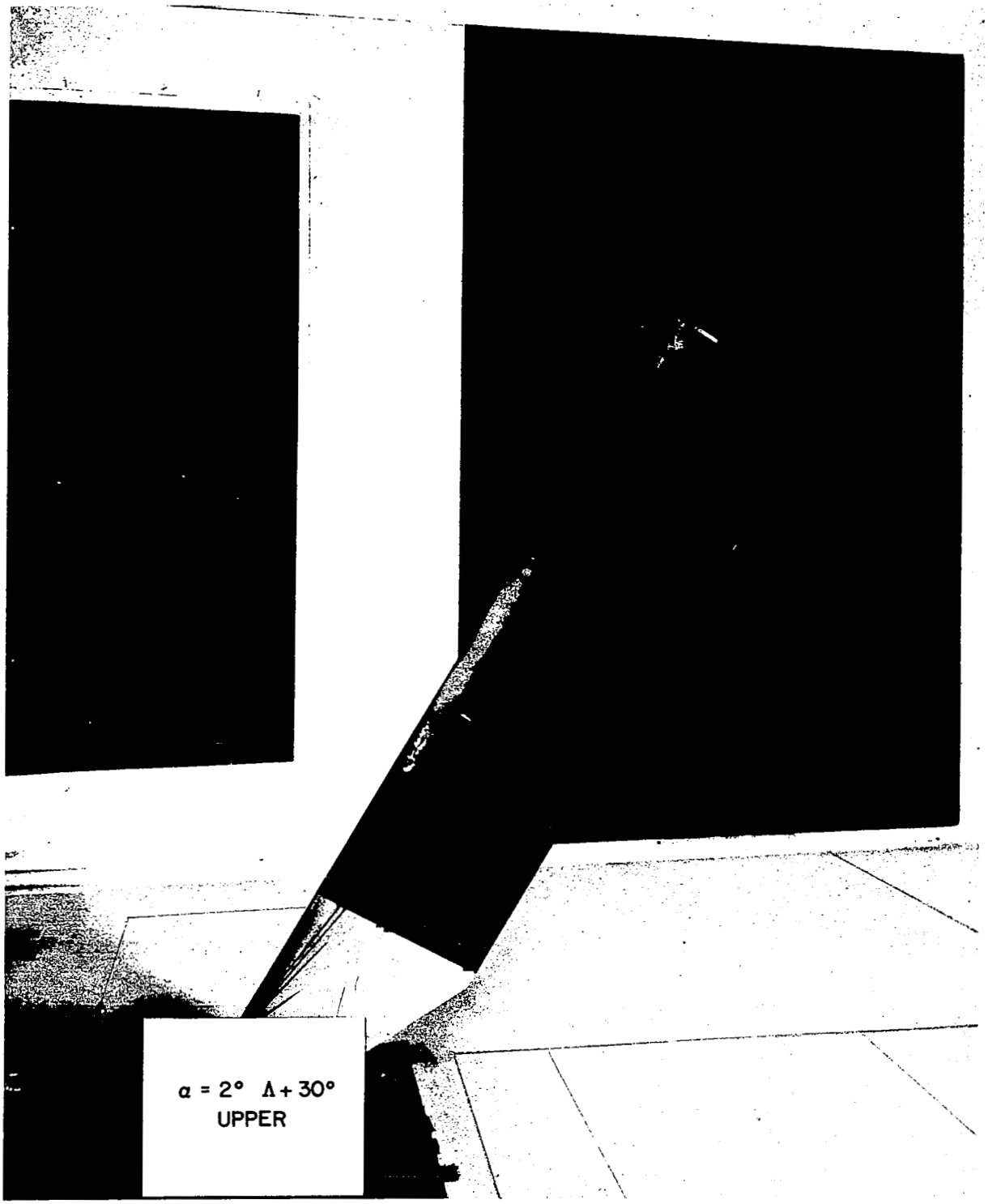

Figure 2.— Representative acenapthane flow visualization results on series 3 blade in the 7- by 10-foot wind tunnel.

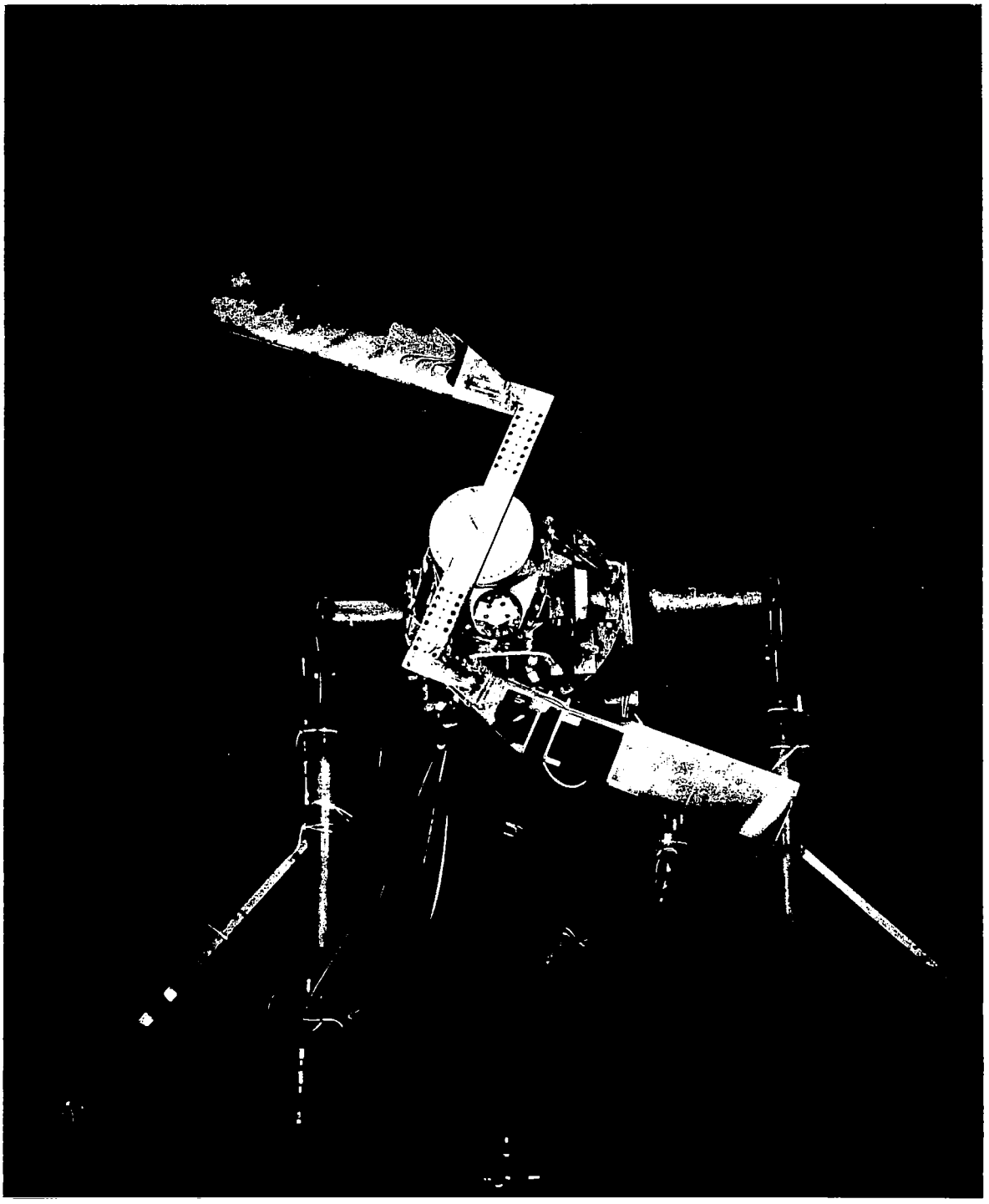

Figure 3.– Series 3 blades mounted in offset configuration on static propeller test stand.

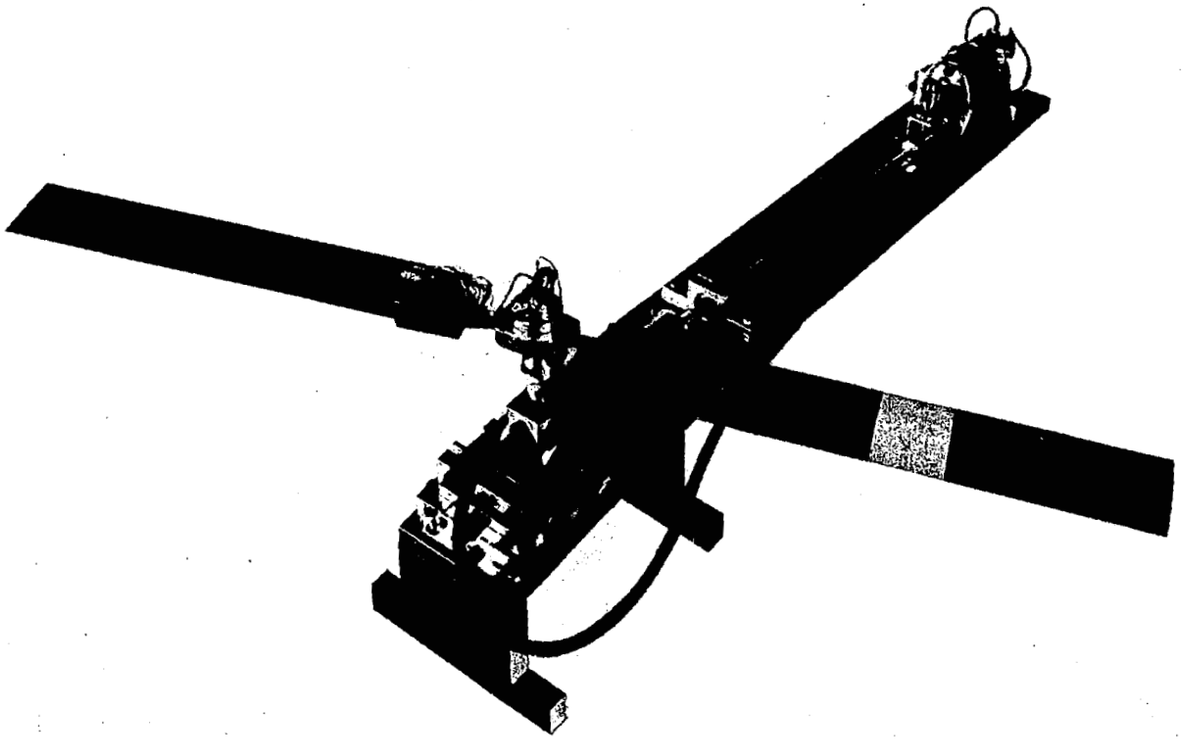

Figure 4.– Series 1 blades mounted on small scale rotor test stand.

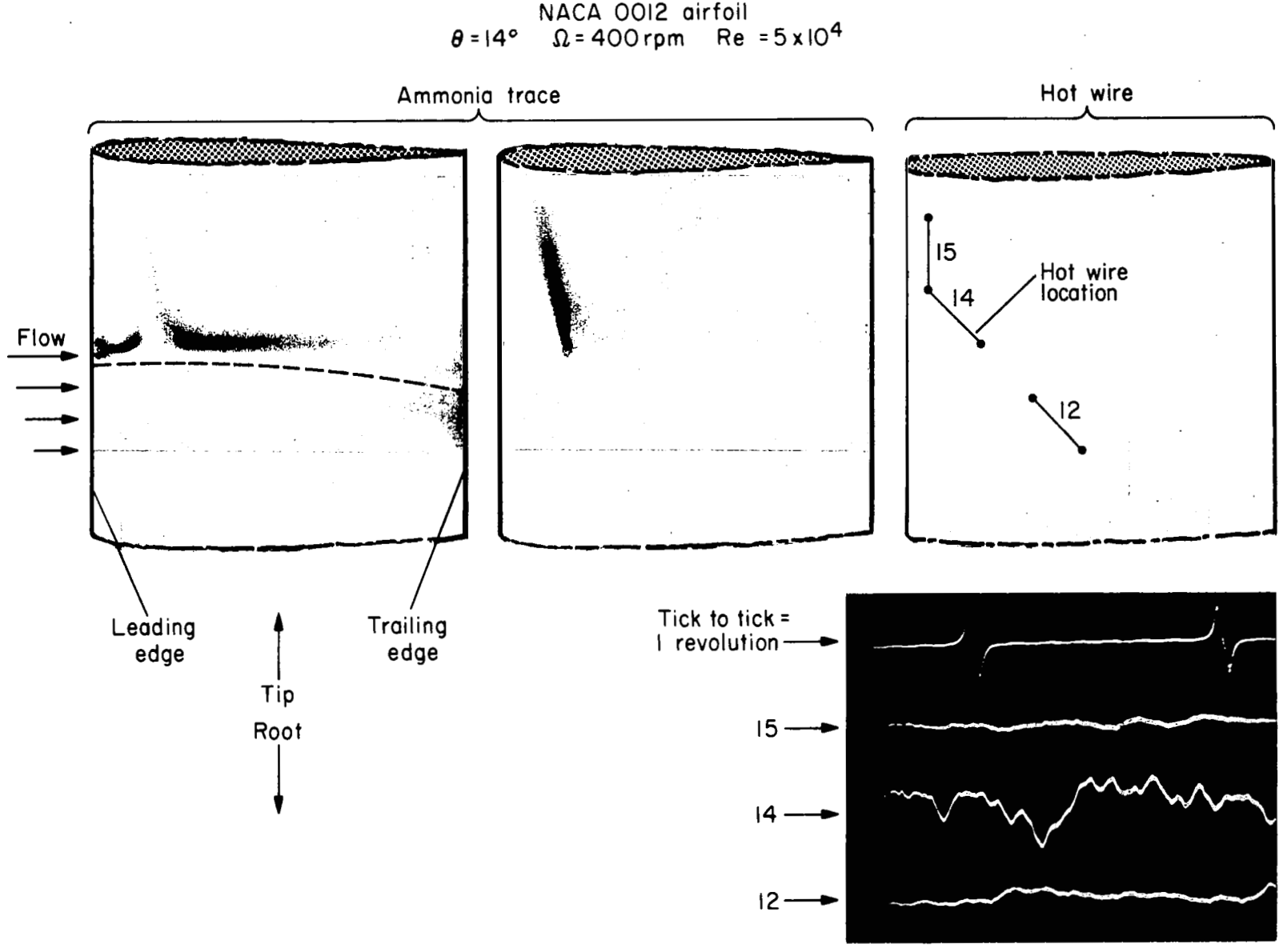

Figure 5.– Hot wire measurements and ammonia trace flow visualization on rotating series 1 blade.

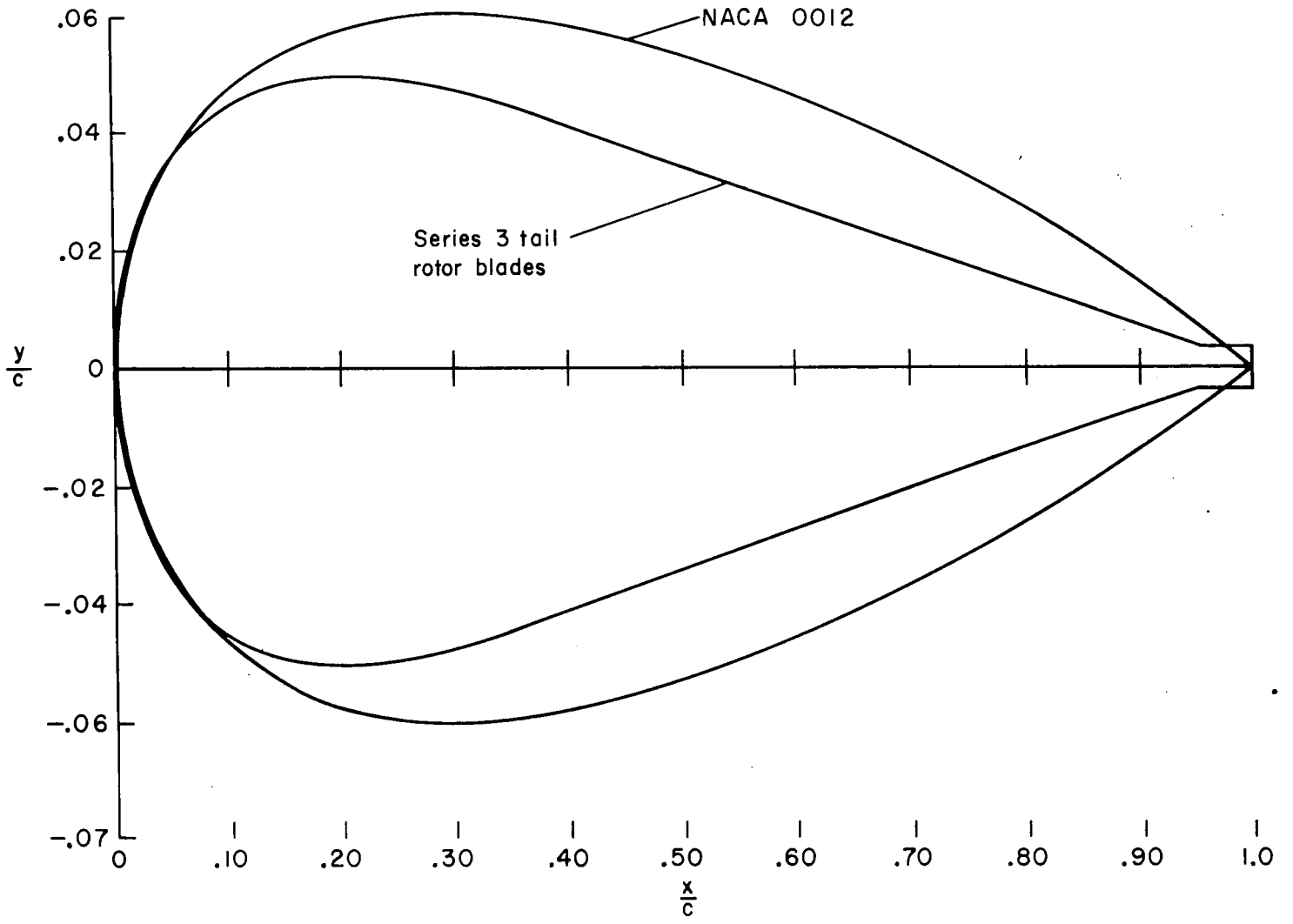

Figure 6.– Airfoil profile shape for series 3 blades.

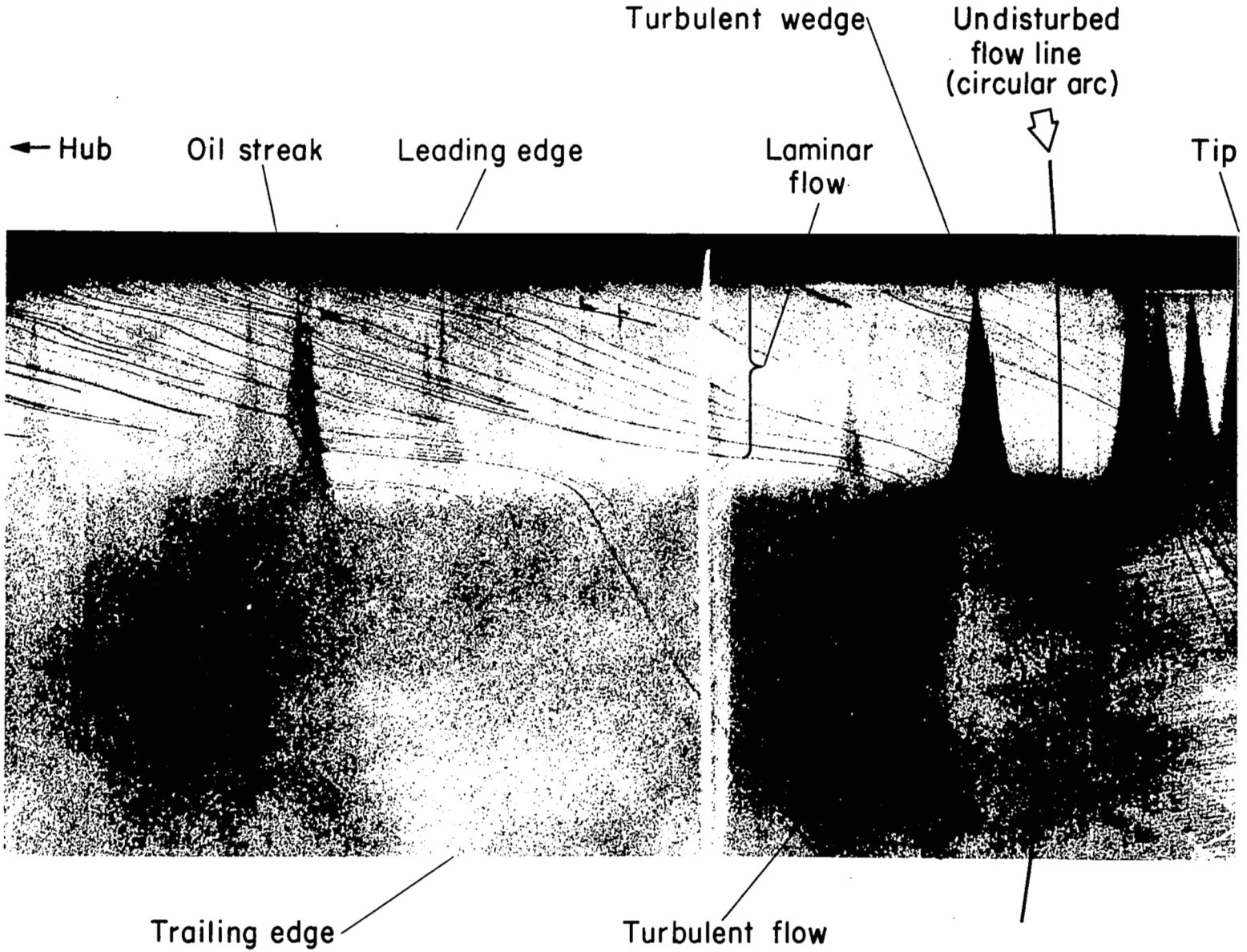

Figure 7.– Oil streak and acenapthane flow visualization on rotating blade at low collective pitch.

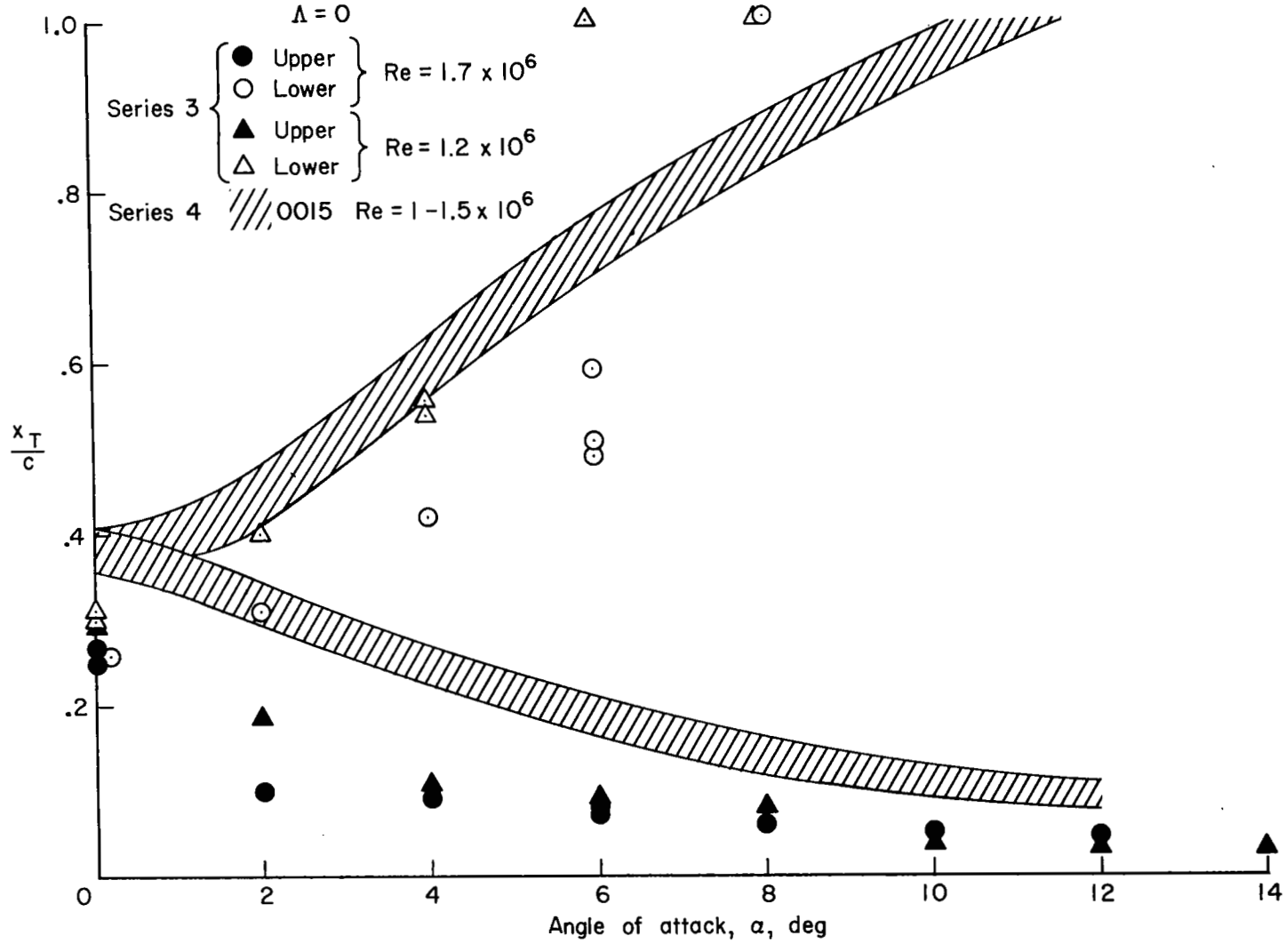

Figure 8.– Chordwise position of transition on nonrotating series 3 and 4 blades at zero yaw.

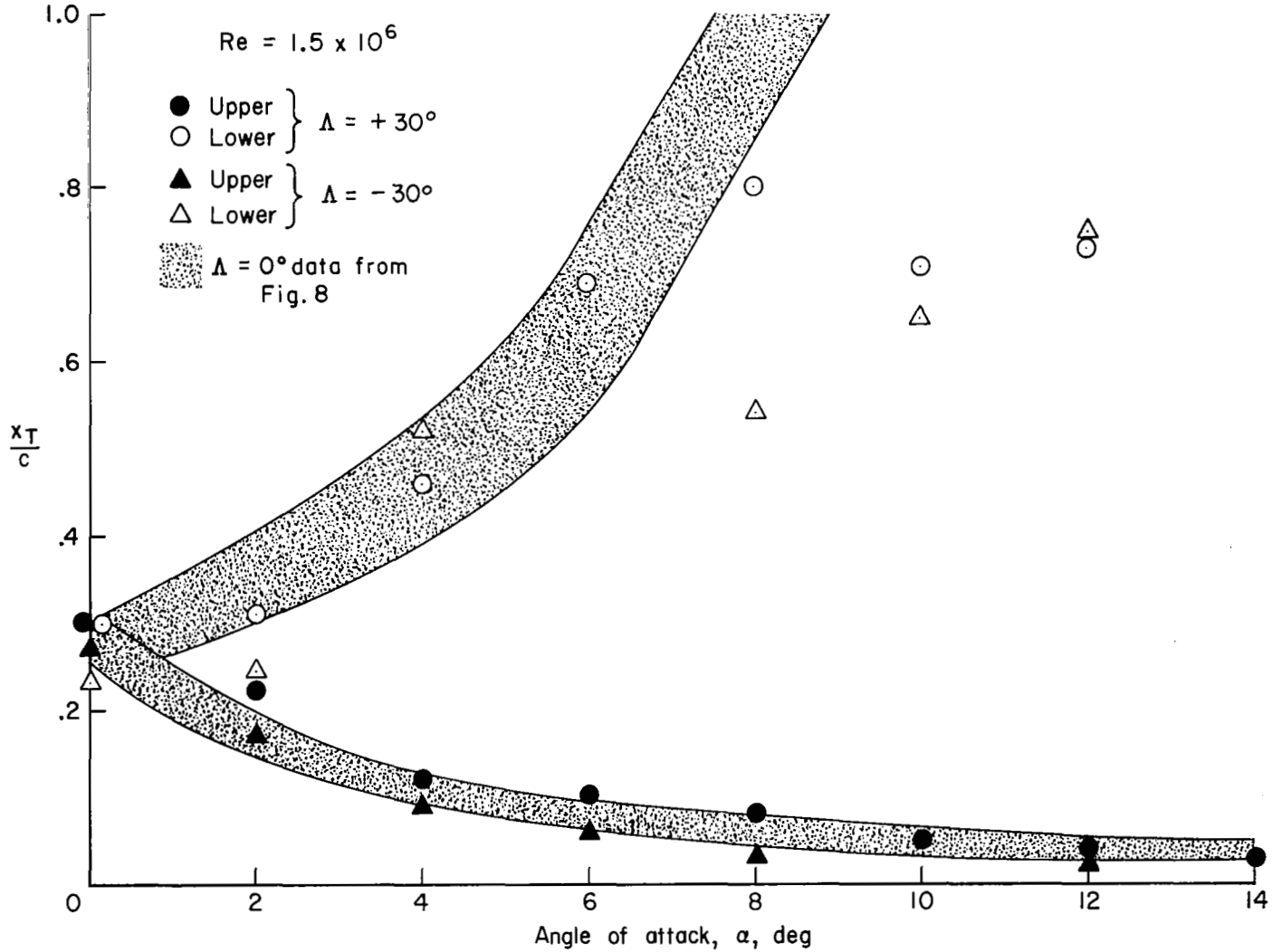

(a) $\Lambda = \pm 30°$

Figure 9.– Chordwise position of transition on nonrotating series 3 blades at various yaw angles.

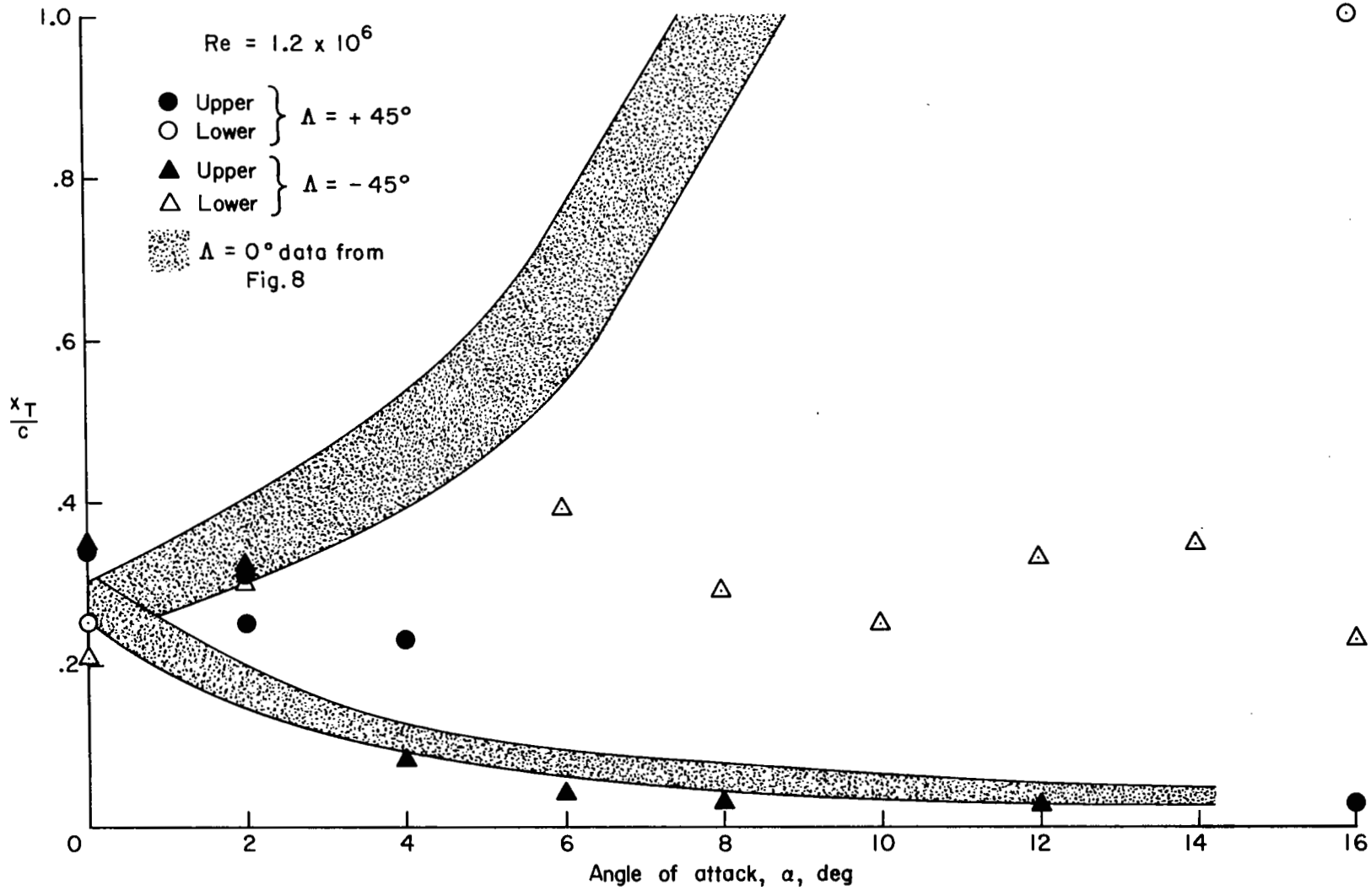

(b) $\Lambda = \pm 45°$

Figure 9.– Continued.

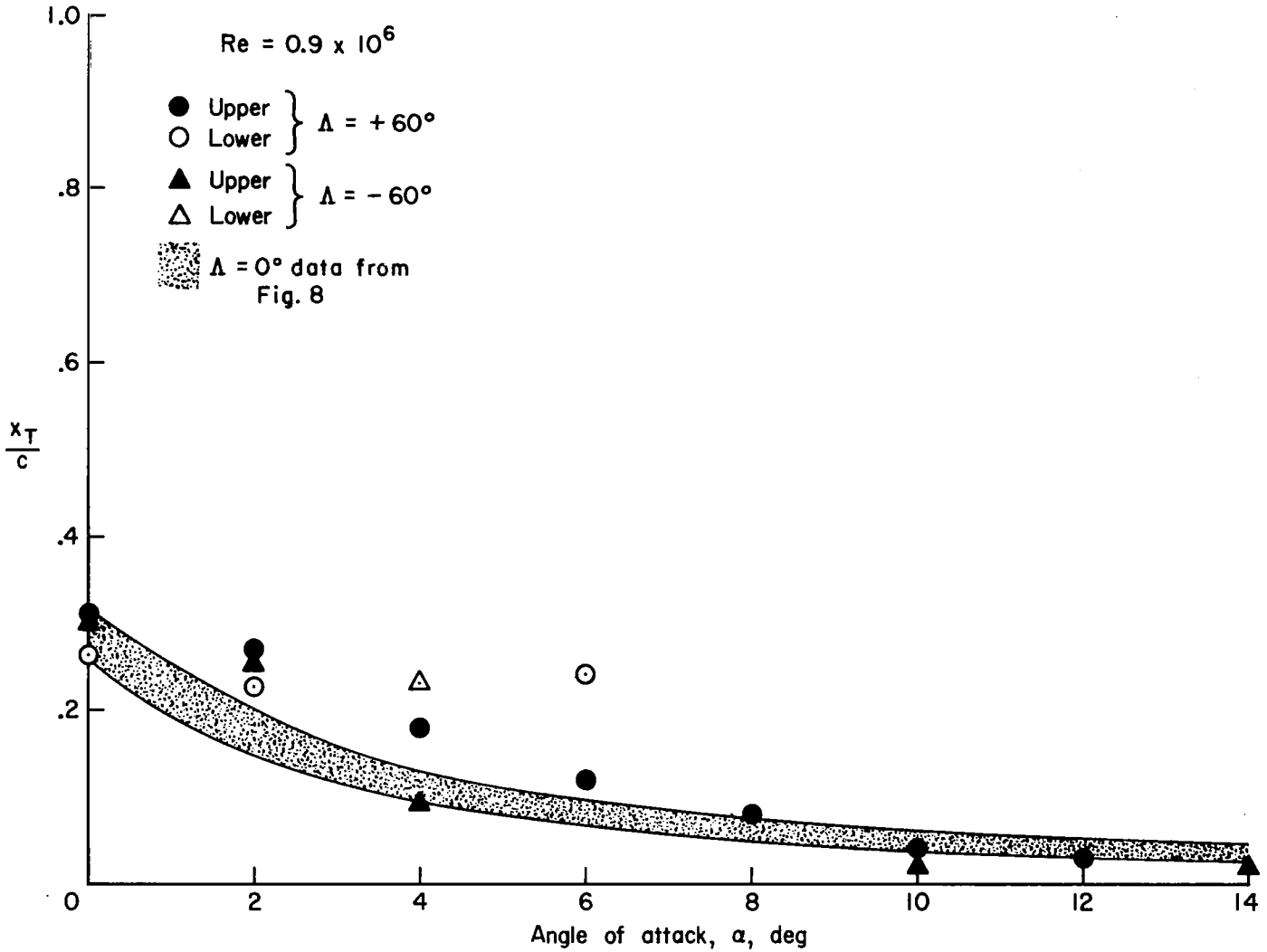

(c) $\Lambda = \pm 60°$

Figure 9.– Concluded.

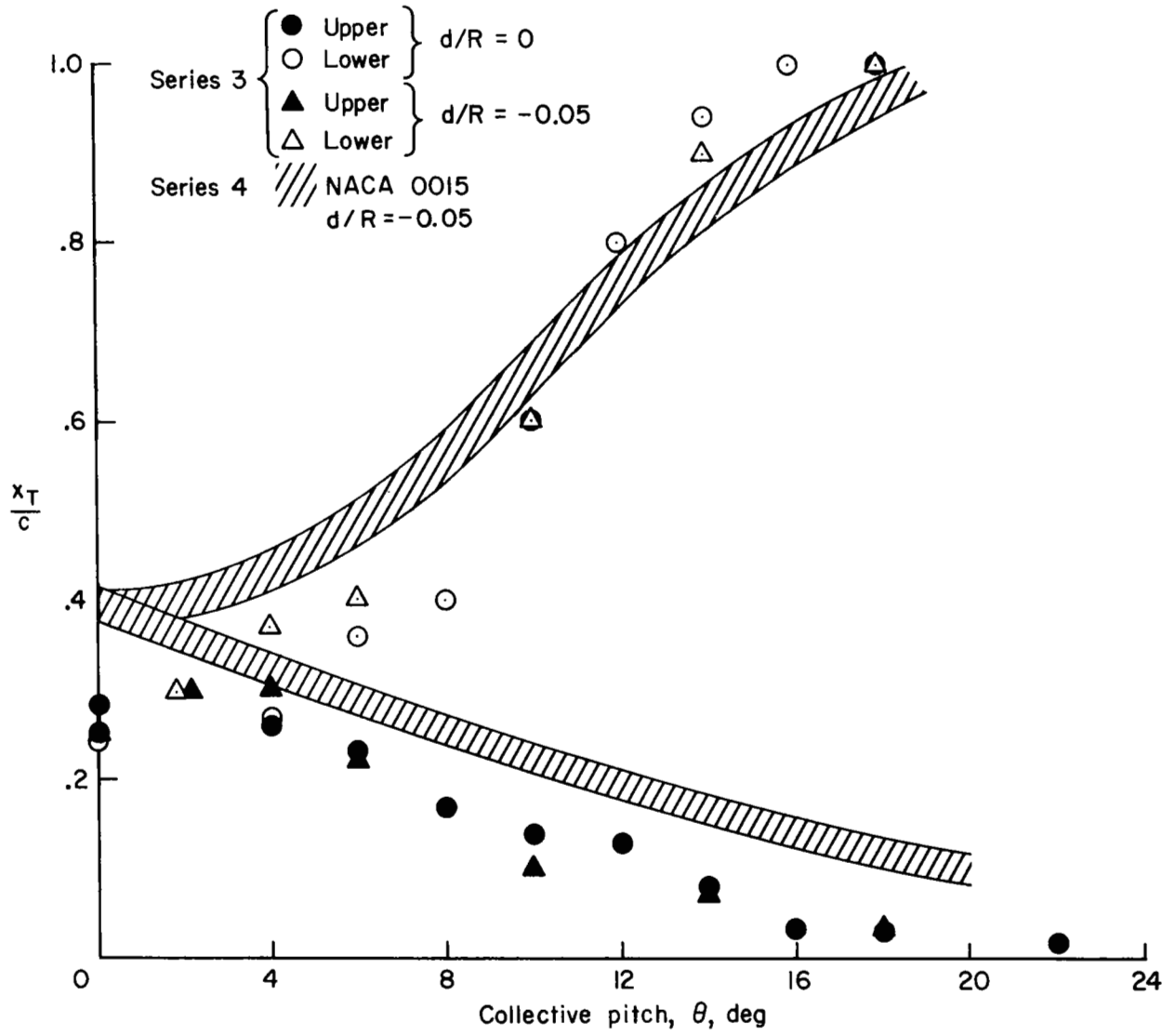

Figure 10.– Chordwise position of transition on rotating series 3 and 4 blades with small offset.

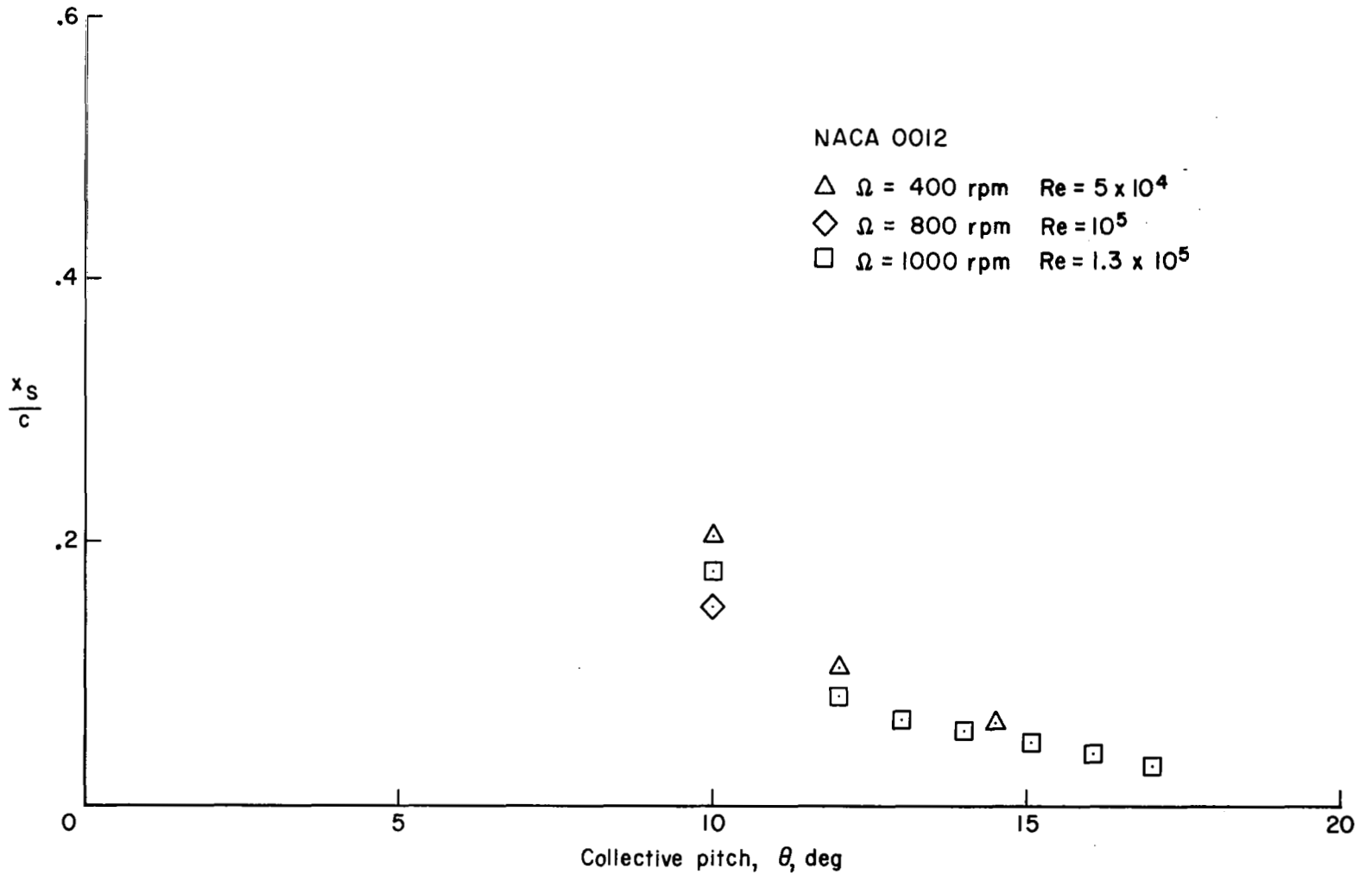

(a) Rotating blades with NACA 0012 airfoil.

Figure 11.– Chordwise position of laminar separation.

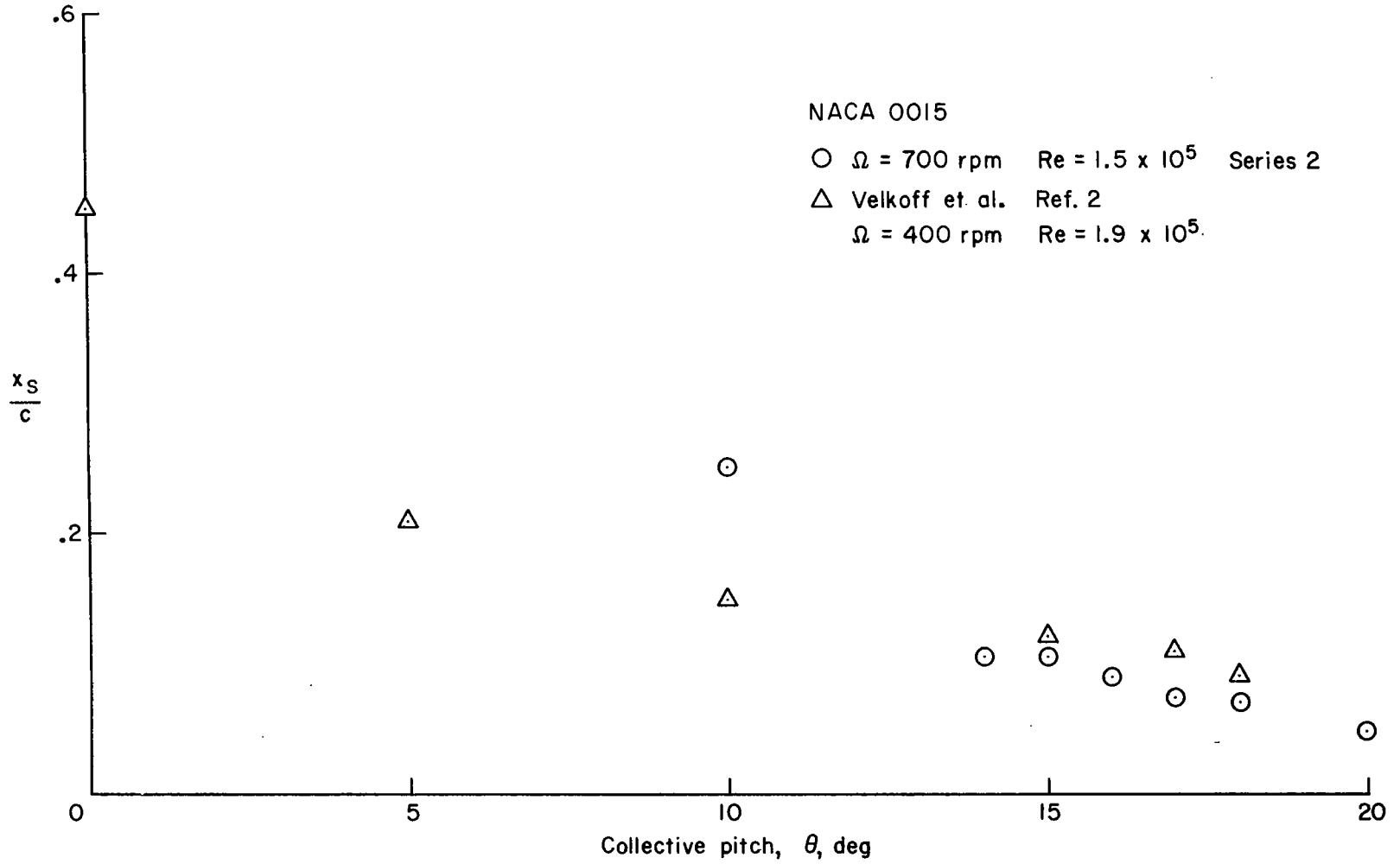

(b) Rotating blades with NACA 0015 airfoil.

Figure 11.– Concluded.

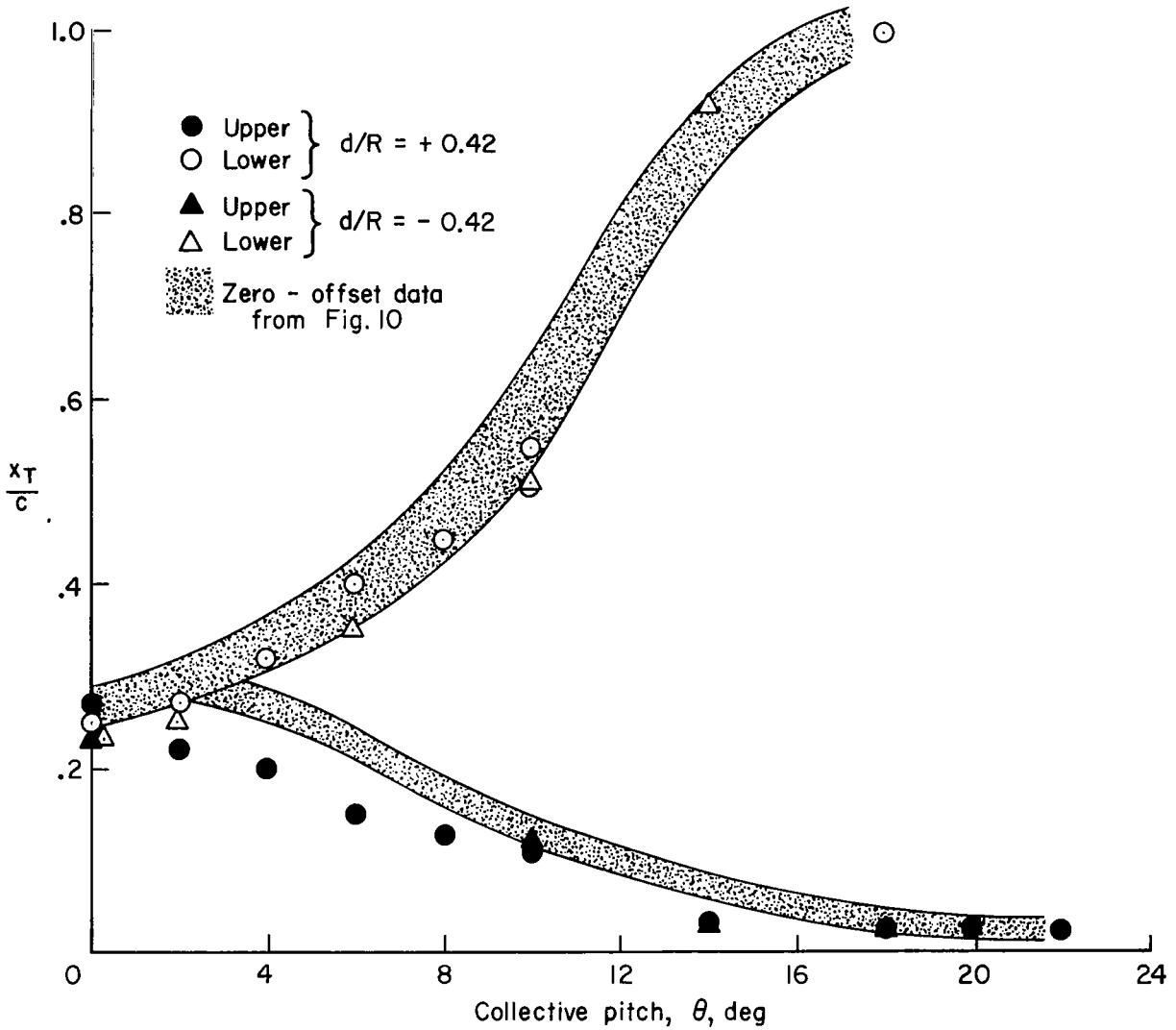

Figure 12.– Chordwise position of transition on rotating series 3 blades with large offset.

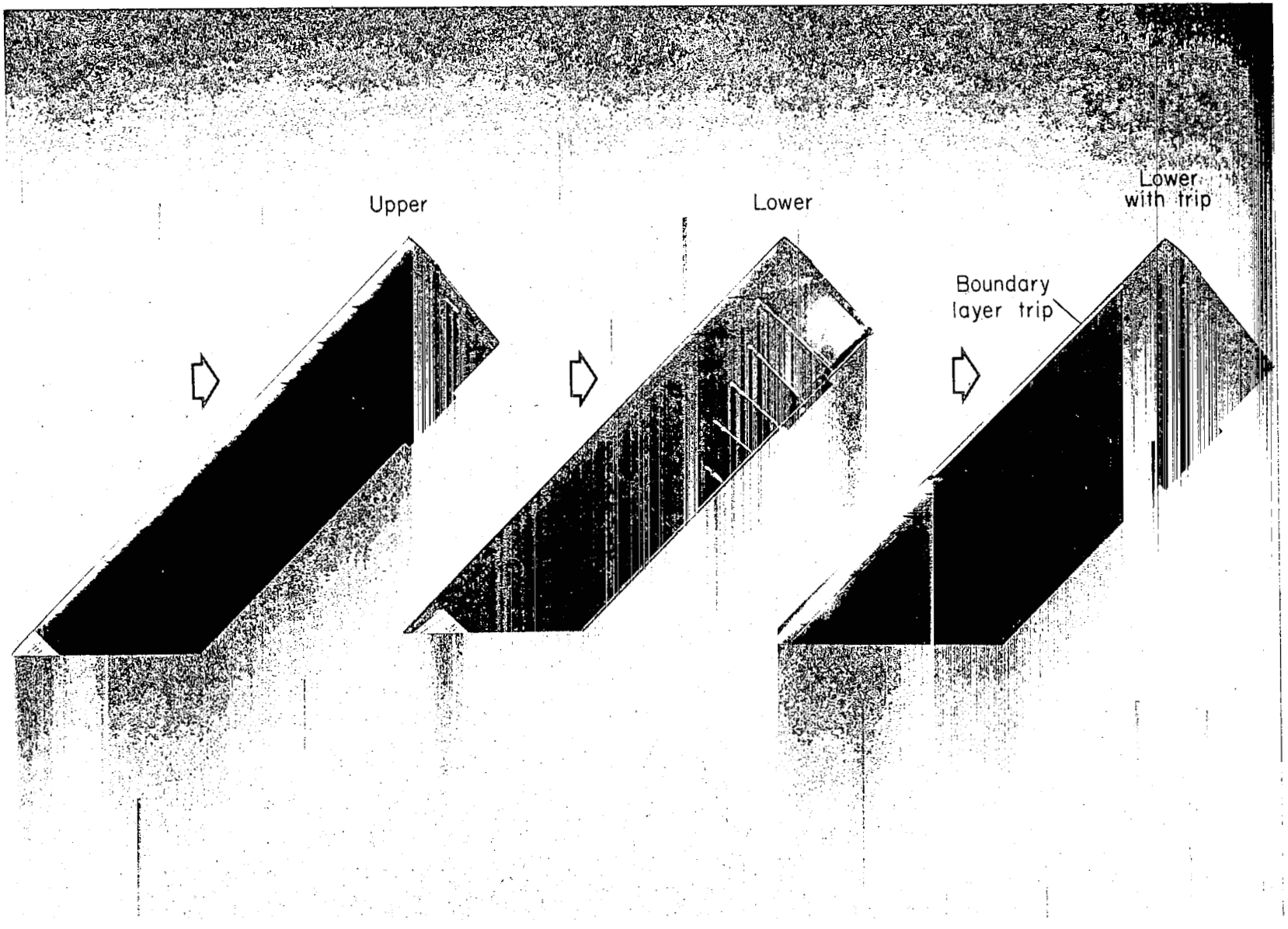

Figure 13.– Acenapthane flow visualization of transition and surface streamline direction on nonrotating yawed blades.

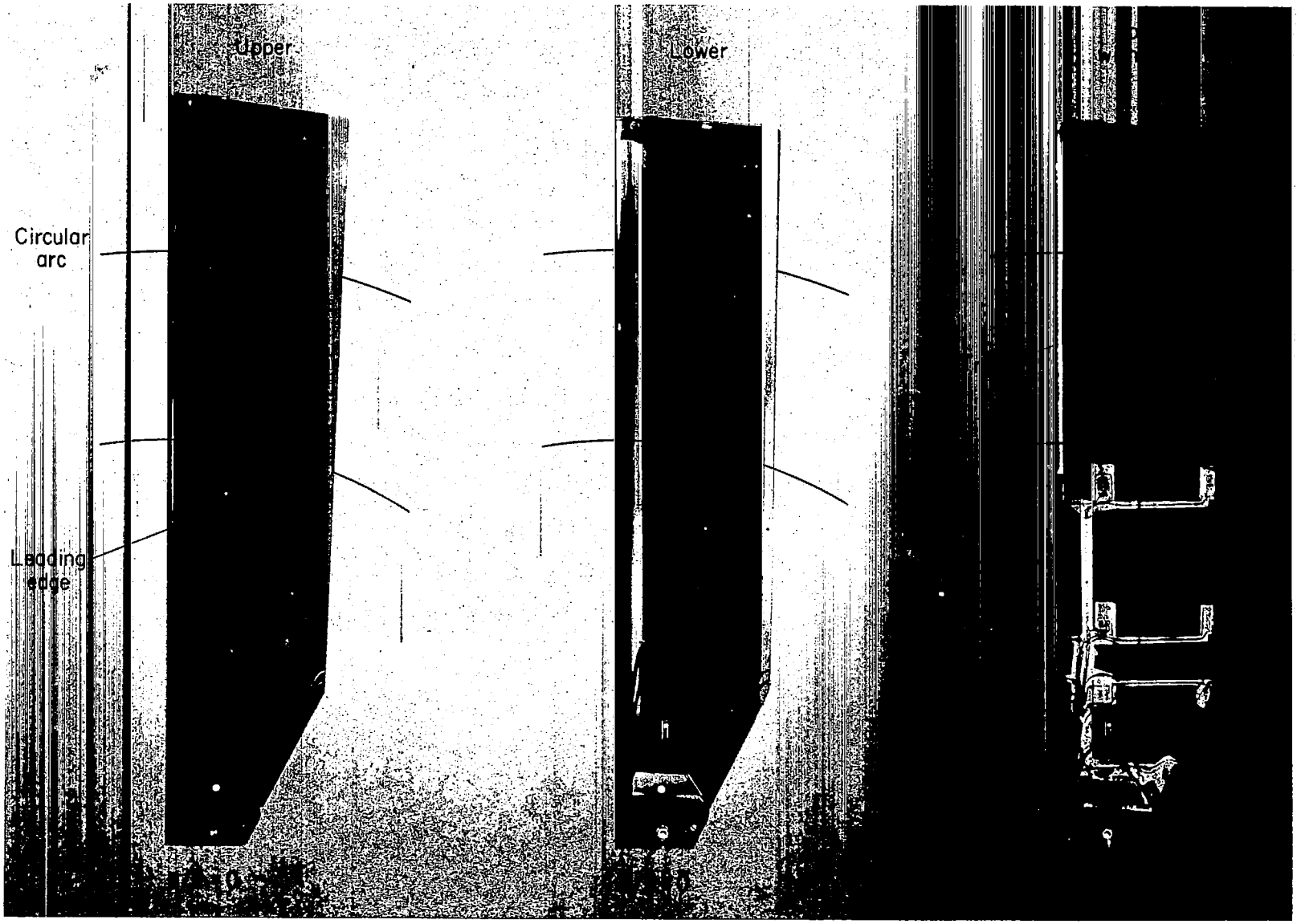

(a) Collective pitch = 2°.

Figure 14.– Flow visualization on rotating blades with conventional offset.

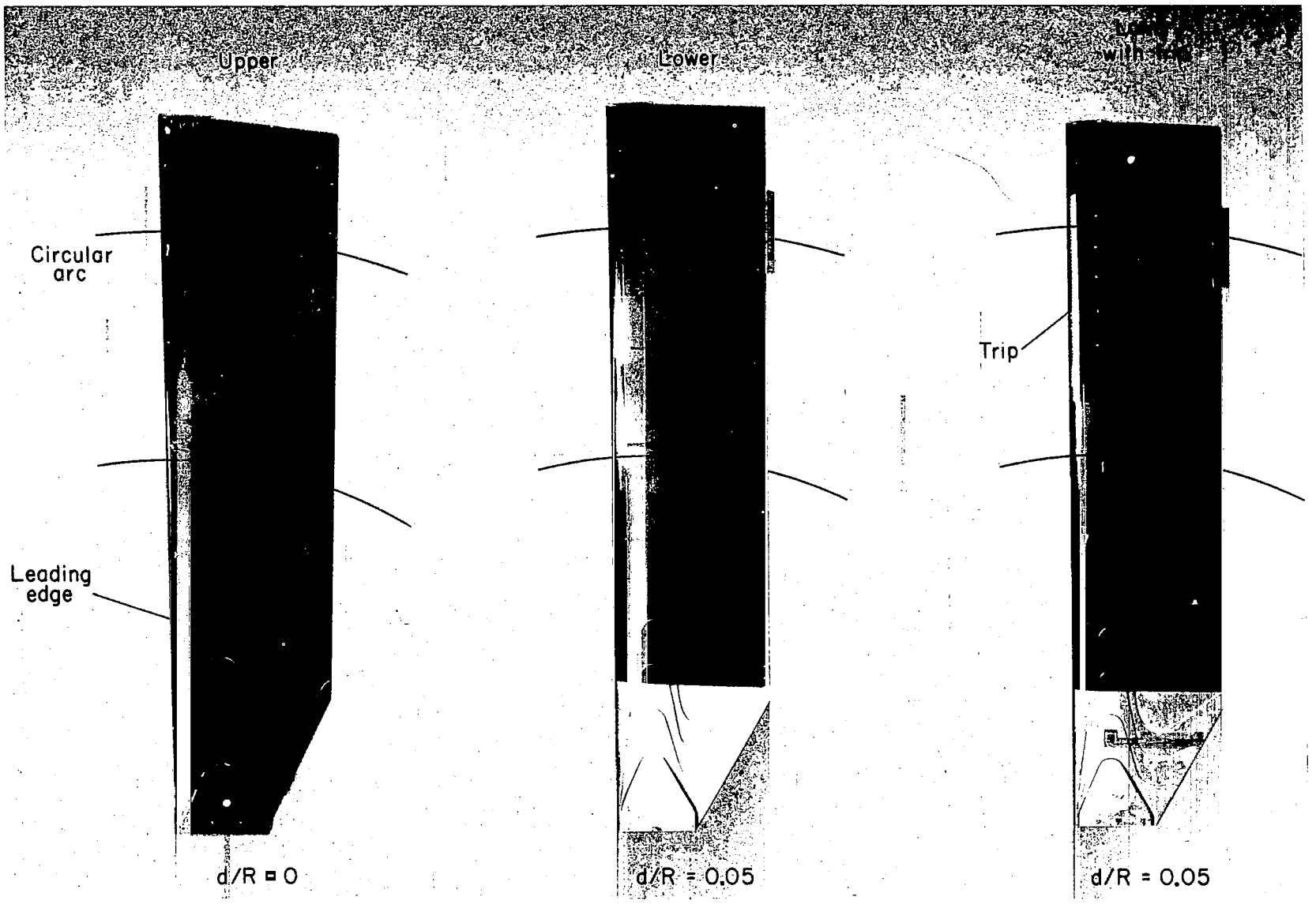

(b) Collective pitch = 10°.

Figure 14.- Concluded.

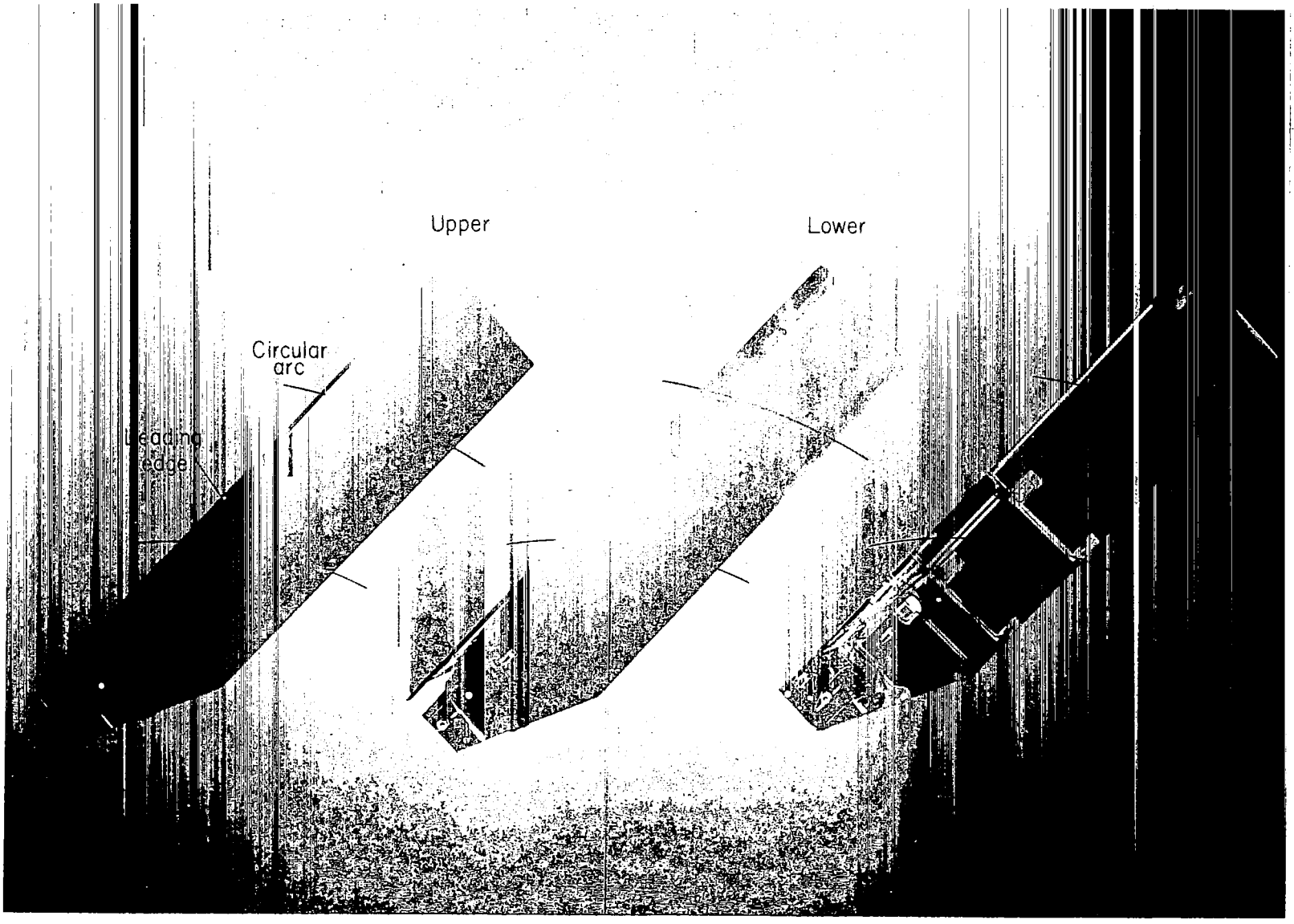

(a) Collective pitch = 2°.

Figure 15.– Flow visualization on rotating blades with large positive offset.

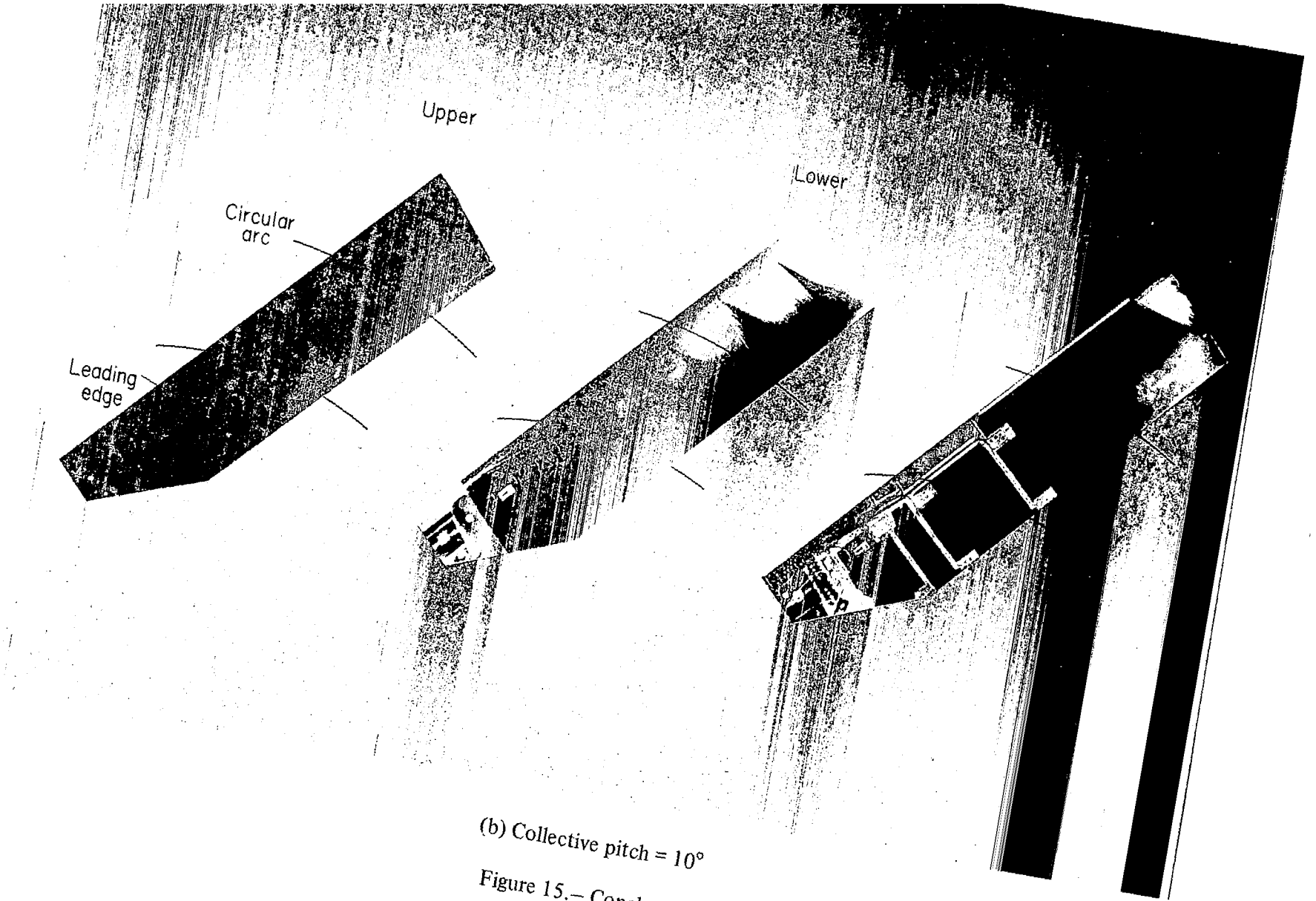

(b) Collective pitch = 10°

Figure 15.– Concluded.

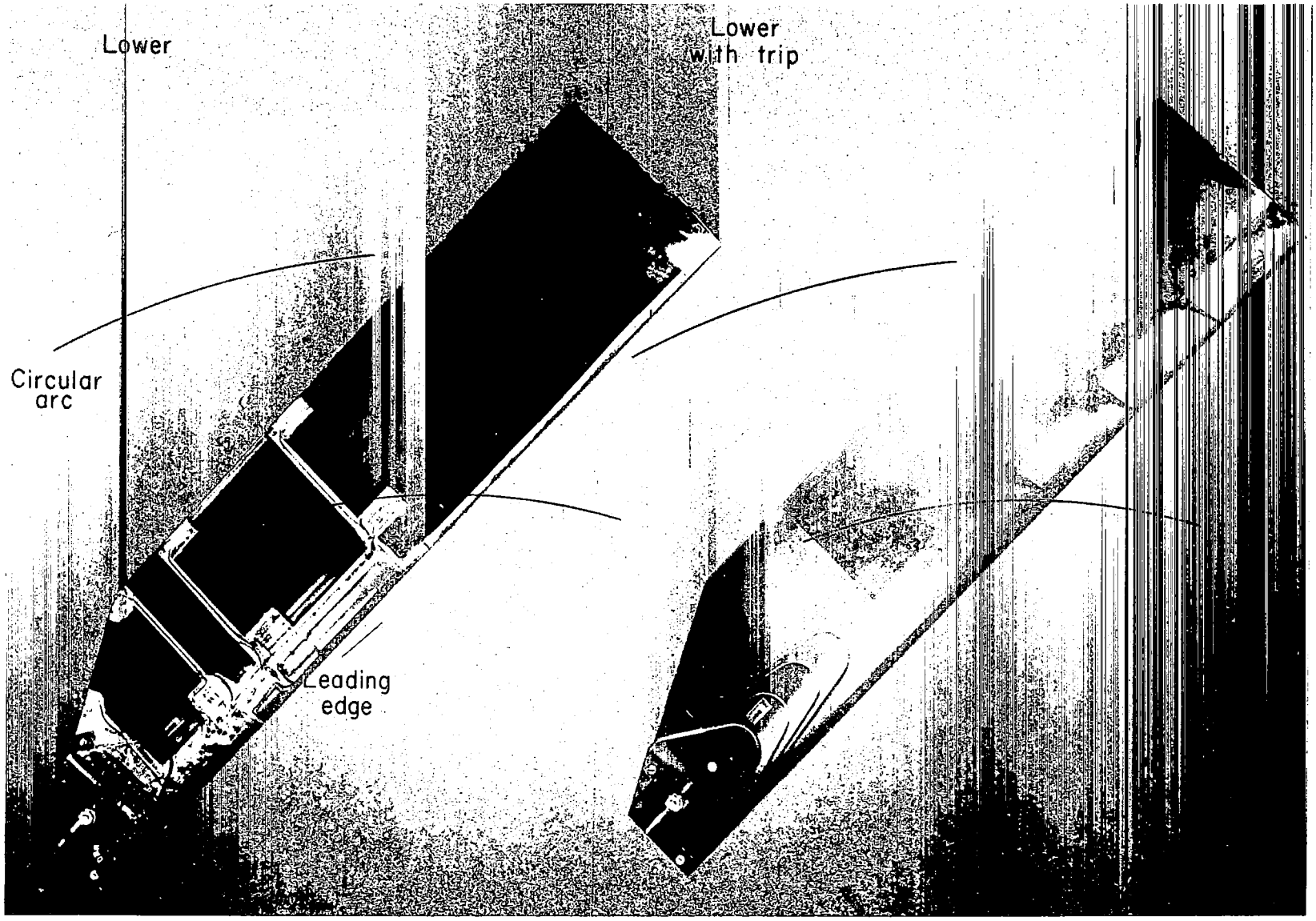

(a) Collective pitch = 2°.

Figure 16.– Flow visualization on rotating blades with large negative offset.

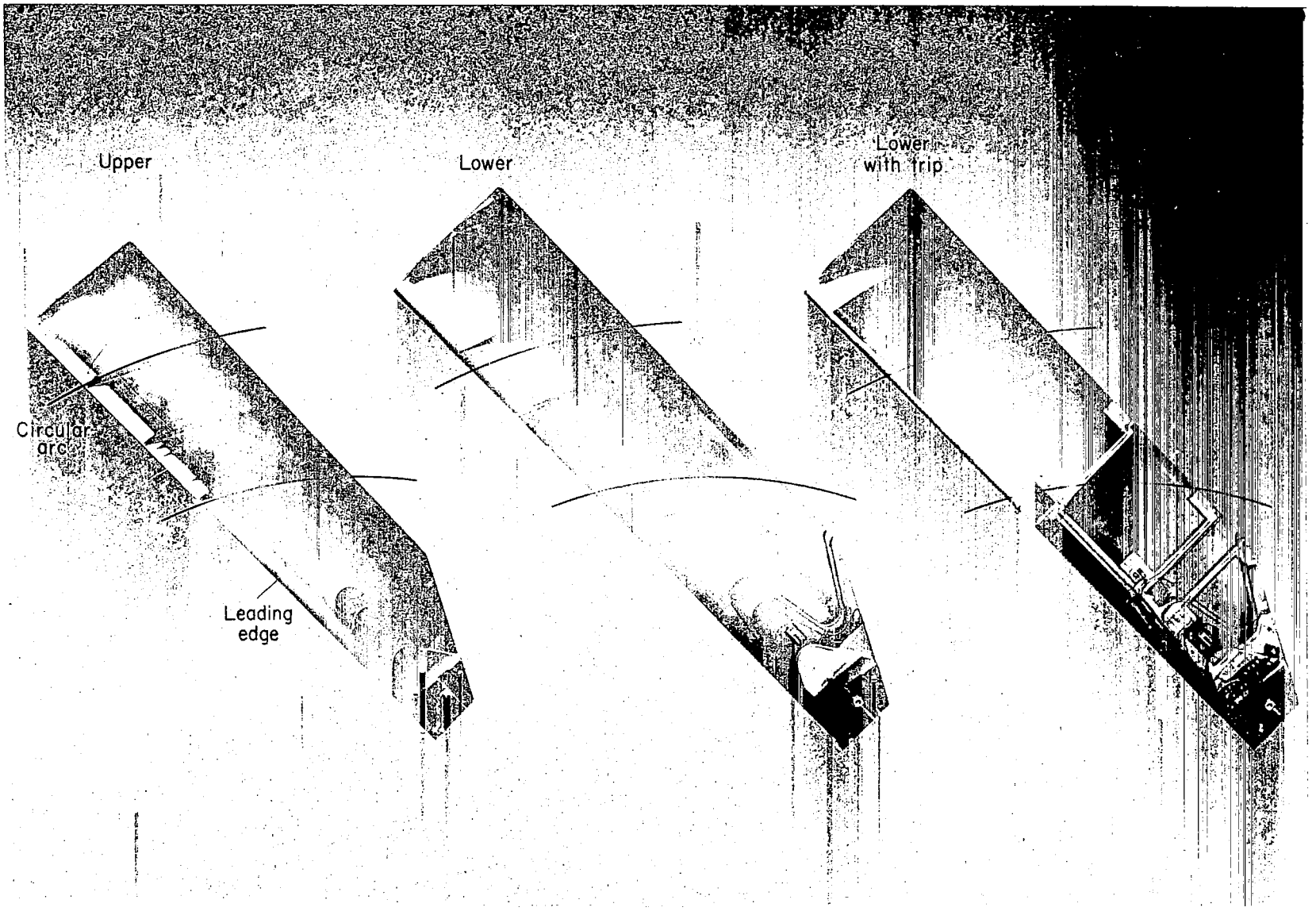

(b) Collective pitch = 10°.

Figure 16.– Concluded.

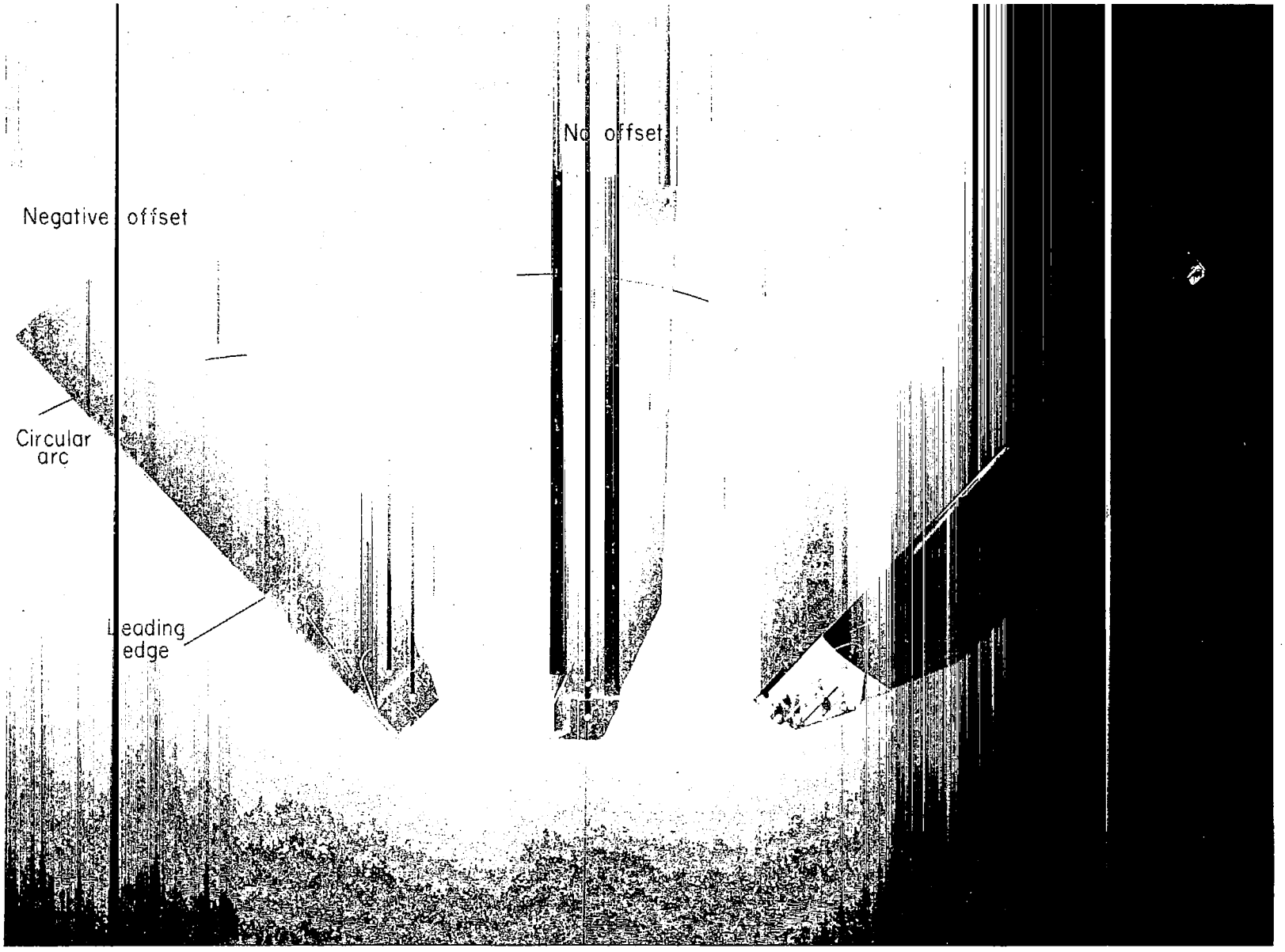

Figure 17.– Flow visualization on rotating blades close to stall for three offset configurations; collective pitch = 22°.

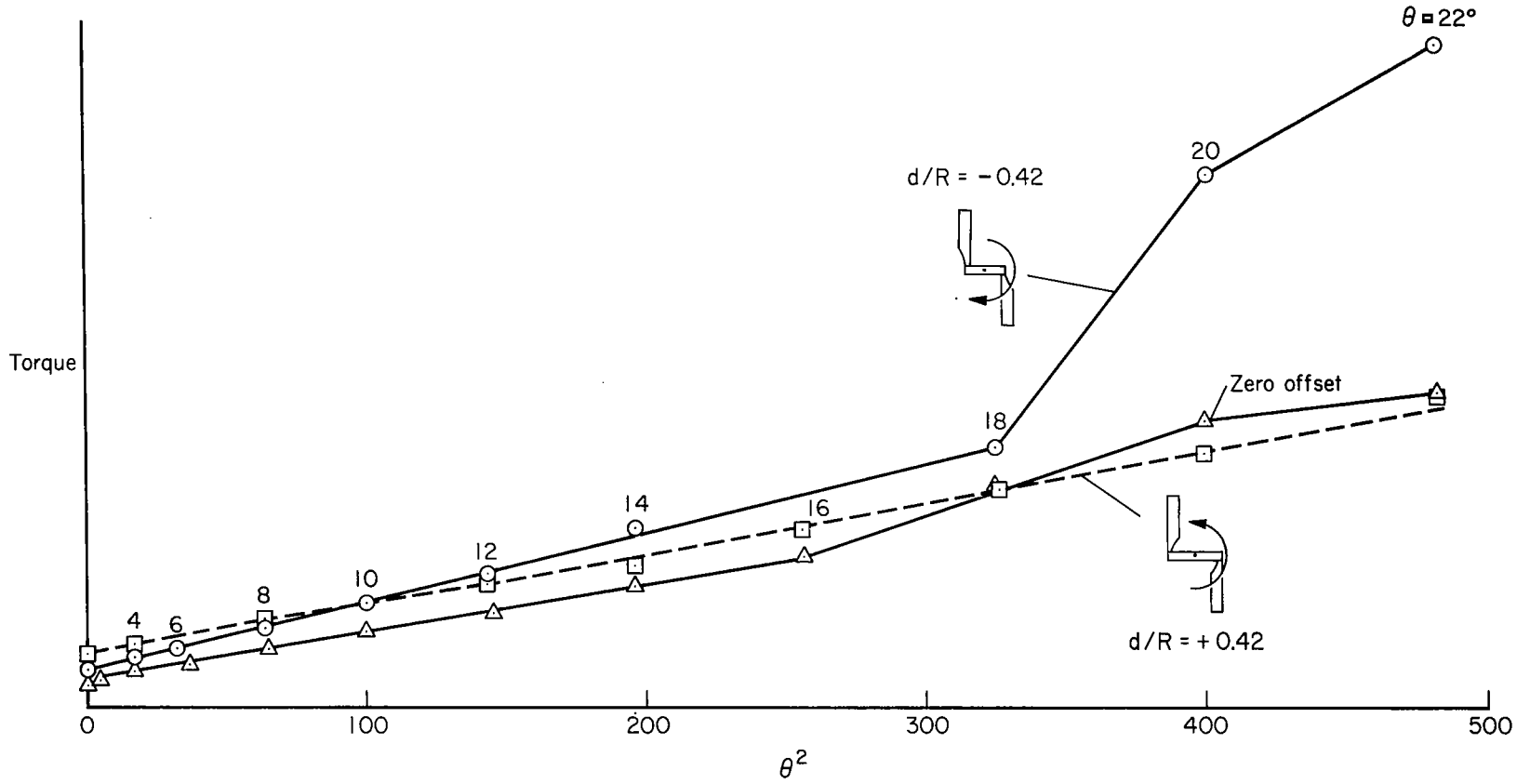

Figure 18.– Variation of rotor torque with collective pitch for three offset configurations.

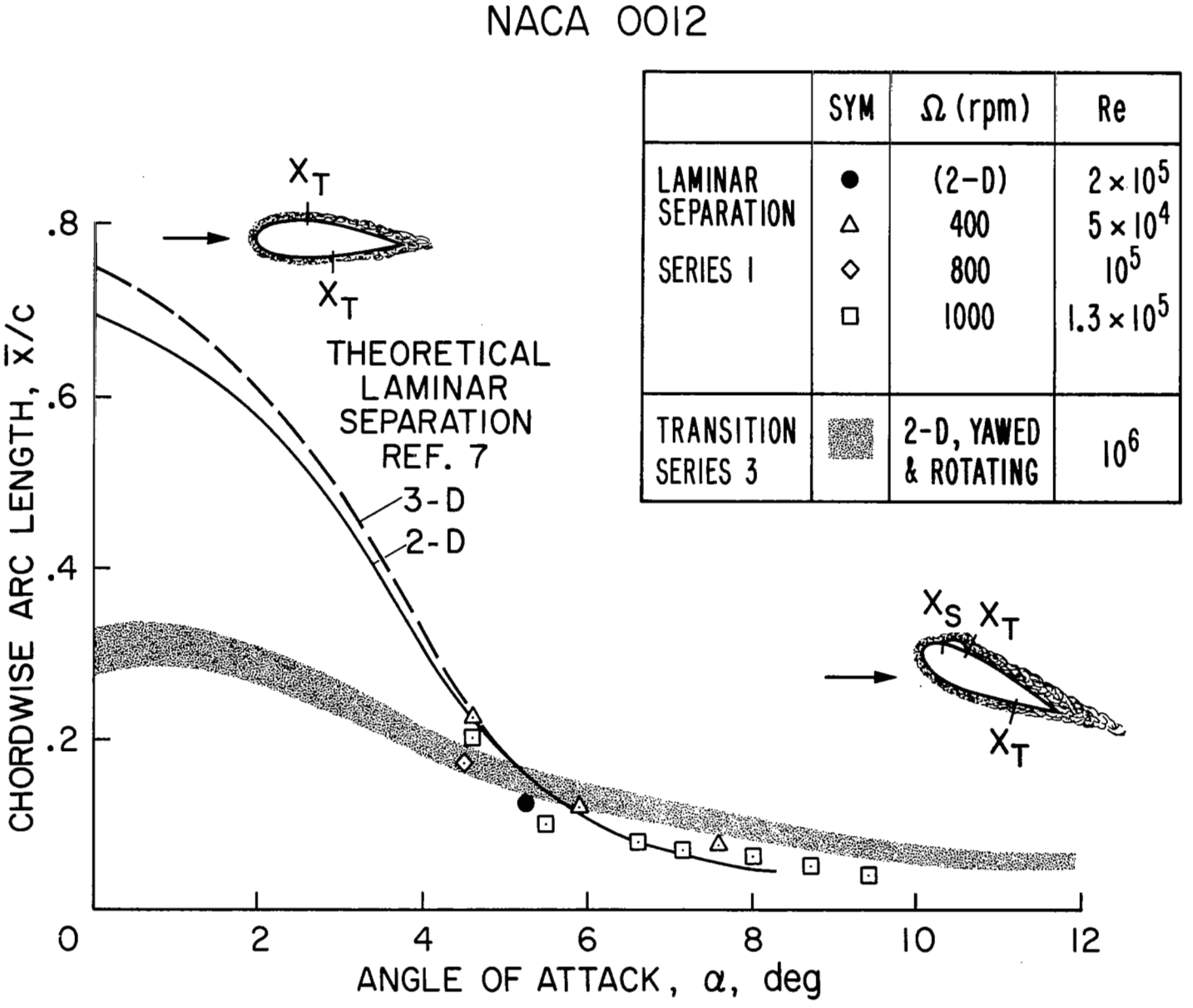

Figure 19.– Summary of separation and transition results on rotating blades with conventional offset.